Uncertainty Quantification of Reactor Simulation Codes Using Collocation-Based Reduced Order Models

by

Artem Yankov

A dissertation submitted in partial fulfillment
of the requirements for the degree of
Doctor of Philosophy
(Nuclear Engineering)
in the University of Michigan
2013

Doctoral Committee:

Professor Thomas J. Downar, Chair
Professor John C. Lee
Professor John P. Boyd

TABLE OF CONTENTS

LIST OF FIGURES

LIST OF TABLES

LIST OF ABBREVIATIONS

PDE partial differential equation

SPDE stochastic partial differential equation

HDMR high-dimensional model representation

ANOVA analysis of variance

TMI Three Mile Island

UAM Uncertainty Analysis in Modeling

PARCS Purdue Advanced Reactor Core Simulator

SCALE Standardized Computer Analyses for Licensing Evaluation

ENDF Evaluated Nuclear Data File

ADFs assembly discontinuity factors

LHS Latin Hypercube Sampling

CHAPTER 1

Introduction

1.1 Overview of Previous Work

Modeling nuclear reactor stability and performance computationally has evolved into a multi-physics and multi-scale regime. Various computer codes have been developed and optimized to model individual facets of reactor operation such as neutronics, thermal-hydraulics, and kinetics. These codes are most often coupled to produce more physical results. While it is crucial to be able to produce best-estimate calculations for the design and safety analysis of nuclear reactors, it is equally important to obtain design margins by propagating uncertainty information through the entire computational process. Replacing seemingly arbitrary design margins based on engineering judgment with design margins based on the uncertainty quantification of computer codes can help overcome significant human shortcomings [16].

The methodologies used for uncertainty quantification in nuclear engineering have generally mirrored the computational resources available during the time of development. When computational resources were relatively limited, methods based on perturbation theory were derived since the method computation times are independent of the number of input parameters [53]. Perturbation theory applies a number of linear approximations and adjoint operators to allow for the retrieval of sensitivity coefficients and basic statistical moments of responses of interest. However, in perturbation theory each desired response requires the solution of a deterministic equation and in some inhomogeneous problems in reactor physics the linear approximations may fail [19]. In addition, application of perturbation theory techniques to computer codes is highly intrusive. Coupled, multiphysics uncertainty analyses using perturbation theory are prohibitive especially when legacy codes are involved. Yet another drawback of perturbation theory in neutronics applications arises in the adjoint-based formulation for cross section uncertainty propagation. In this case, exceptions must be made to responses that cannot be expressed as ratios of reaction rates,

as in the transport cross section and assembly discontinuity factors (ADFs) [60] [59].

As computer resources increased, the linear approximations of perturbation theory were gradually relaxed until routine Monte Carlo sampling became feasible. In the XSUSA method a 44-group covariance matrix is stochastically sampled to generate perturbed few-group cross sections that can be used as input to a Monte Carlo uncertainty analysis in a core simulator [37]. While uncertainty quantification using Monte Carlo sampling does not apply any approximations to the mathematical system under investigation, the computational expense is tremendous, and the extraction of information such as sensitivity coefficients can be difficult. Nevertheless, sampling provides a brute force means by which many uncertainty quantification algorithms can be validated.

Recently, an approach based on the stochastic finite element method, referred to as polynomial chaos expansion, has been developed for the purposes of uncertainty quantification [22]. The basic idea behind polynomial chaos expansions is to expand the random variables of some governing stochastic partial differential equations in terms of orthogonal polynomials and then to apply Galerkin projections [43]. This idea is similar to the angular expansion of the scatter cross section in terms of Legendre polynomials in neutron transport theory. Methods for uncertainty quantification that employ polynomial chaos expansions fall under the general mathematical framework of spectral methods. The motivation behind spectral methods, and specifically collocation, for uncertainty quantification is to combine the rapid convergence rates of deterministic methods with the generality of stochastic sampling methods.

While used extensively in structural and materials engineering, polynomial chaos expansions have been seldom applied in nuclear engineering. In [57] and [56] the author applies analytic polynomial chaos techniques to investigate the effect of random material properties on radiation transport through a slab in the P1 approximation. The authors in [4] apply non-linear polynomial chaos to examine static and dynamic eigenvalue uncertainties due to uncertainties in cross section values. Finally, the authors in [17] use polynomial chaos-collocation to study the effects of total cross section uncertainties on the probability density function of the scalar flux in absorbing and diffusive media.

The polynomial chaos expansions based on stochastic Galerkin methods applied in the research above exhibit several substantial advantages over Monte Carlo and perturbative methods. Mainly, spectral convergence rates can be achieved. In addition, while nonlinearities and large uncertainties in random variables pose problems for perturbation methods, the stochastic Galerkin methods easily deal with such factors. However, the primary drawback of polynomial chaos expansions with stochastic Galerkin methods lies in their intrusive nature. In other words, unless an engineering code is initially developed with

stochastic Galerkin capabilities, which is unlikely, extensive modifications will have to be made to the code. Modifications include adding the ability to solve an enlarged system of coupled, partial differential equations.

To this end the stochastic collocation method, a variant of polynomial chaos expansion, is considered since it circumvents the need to modify engineering code in order to implement spectrally converging uncertainty quantification methods. Stochastic collocation methods are essentially interpolatory, projecting a set of deterministic simulations onto a polynomial basis. With stochastic collocation codes can be treated as "black boxes". Such an attribute is highly desirable for the uncertainty analysis of nuclear engineering computer codes since often these consist of coupled, multi-physics, and multi-scale legacy code. The success of perturbatory methods, which are linear, in the uncertainty analysis of nuclear engineering codes is indicative of the potential for stochastic collocation. Being a spectral method, stochastic collocation performs best on smooth functions [10].

However, even when utilizing a stochastic collocation method based on sparse grid constructs, the method suffers from the so-called "curse of dimensionality" [43]. The "curse of dimensionality" arises when the convergence of a method is proportional to the exponent of the the function's dimensionality, as in a full tensor product interpolation scheme. While sparse grids help to mitigate the "curse of dimensionality" researchers have shown that when applied to realistic engineering computer simulations the practicality of stochastic collocation diminishes for dimensions greater than $\mathcal{O}(10)$ [42]. Consequently, further mitigation is needed in order to apply stochastic collocation to real-world engineering problems. To this end, reduced order models, also known as surrogate models, are utilized. Reduced order models work to find a relatively small subspace of some function that is still representative of the original function space.

Performing uncertainty quantification on high-dimensional, coupled, multiphysics engineering codes can be prohibitive if the codes take many hours to run. To make uncertainty quantification feasible for such problems reduced order models are constructed. While a reduced order model may be computationally expensive to build, the ideal end product is a function that can be rapidly evaluated while simultaneously preserving the predictive capabilities of the large-scale model [11]. Due to the rapid evaluation of the reduced order model, uncertainty quantification, optimization studies, probabilistic analysis, and inverse problems can be carried out.

The popularity of collocation-based methods for uncertainty quantification have stemmed from greater accessibility to computing clusters. As recently as 2006 the theme in uncertainty quantification had been how to get the most out of a limited number of available simulations [25]. In [25] researchers investigated whether it is more accurate to estimate

statistics directly from N unstructured simulations of a large-scale engineering code or from a trend model based on the N simulations. Krigging interpolation and multivariate adaptive regression splines are two common approaches for building trend models [50]. Collocation methods differ from such response surface approximation methods mainly in their use of structured grids at which the large-scale codes are evaluated. Use of structured grids generally allow for faster convergence to various error thresholds. However, to achieve the expected convergence of collocation algorithms the number of times a large-scale code must be executed is dictated by the algorithm and not the user.

1.2 Stochastic Partial Differential Equations

A stochastic partial differential equation (SPDE) is similar in flavor to the better known partial differential equation (PDE), the main difference being the presence of input uncertainties in the former's parameter space. If the parameters in some PDE are probabilistic and the affects of those variable parameters on the outputs are of interest, then the PDE must be reformulated into a SPDE. The following example aims to elucidate the difference between PDEs and SPDEs and to motivate a discussion of the unique features characteristic to SPDEs. While these features form the mathematical back-bone for this thesis they are somewhat abstract and not crucial to developing an understanding of the subject matter.

Consider the PDE describing one-speed diffusion of neutron flux in a slab nuclear reactor [15]:

$$\begin{aligned} \frac{1}{v}\frac{\partial \phi}{\partial t} - D\frac{\partial^2 \phi}{\partial x^2} + \Sigma_a \phi(x,t) &= \nu\Sigma_f \phi(x,t) \\ \phi(x,0) &= \phi_0(x) \\ \phi(a,t) &= \phi(-a,t) = 0 \end{aligned} \tag{1.1}$$

The PDE in 1.1 can be solved for the flux ϕ as a function of both space x and time t. However, such a solution assumes that the parameters in the PDE, namely v, D, Σ_a and $\nu\Sigma_f$, are fixed values. What would happen to the flux if these parameters were described by probability distributions? The flux would be influenced by perturbations to any of the parameters and so the initial two-dimensional problem is converted to a six-dimensional problem, uncertainty in initial and boundary conditions aside. How would the solution to this SPDE be found? A few preliminaries are in order.

1.2.1 Preliminaries

Most of the language used to describe SPDEs comes from the field of probability theory, which is based on the ideas of sets, fields, and events. The notation and definitions described here come mainly from [46]. The ultimate purpose of introducing the proceeding ideas from probability theory is to be able to understand random variables and the Doob-Dynkin Lemma. Some of the jargon used to describe sets will also be utilized when discussing dimension-wise function decompositions. A *set* is simply a collection of objects while a *subset* is a collection of objects contained within the larger set. A *sample space* is the set of all outcomes of an experiment and is usually denoted by Ω. For example, if the experiment is flipping a fair coin then the sample space is $\Omega = \{H, T\}$. Subsets of Ω are referred to as *events*. If $\Omega = \{\omega_1, \omega_2, ..., \omega_N\}$ then the total number of subsets of Ω is 2^N, where both the empty set $\emptyset$ and all of Ω are included in the count.

A few definitions from set algebra are required before moving on to the Doob-Dynkin Lemma. A *union*, or sum, of two sets A and B is the set of elements that are in at least A or B and is denoted by $A \cup B$. The *intersection* of sets A and B consists of all the elements belonging to both A and B and is denoted by $A \cap B$. Finally, the *complement* of a set A, denoted by A^C, consists of all the elements not in A. From these definition, it follows that $A \cup A^C = \Omega$ and $A \cap A^C = \emptyset$.

Now, let's use the ideas of sets, unions, and intersections to define what is meant by a field and sigma field. Let A and B be subsets of the set Ω. The subsets A and B form a *field* M if,

- $\emptyset \in M$, $\Omega \in M$
- If $A \in M$ and $B \in M$ then $A \cup B \in M$ and $A \cap B \in M$
- If $A \in M$ then $A^C \in M$

A *sigma field* $\mathscr{F}$ is a field that is closed under any countably infinite set of unions and intersections. In other words if subsets $A_1, ..., A_n, ...$ belong to $\mathscr{F}$ then so do $\bigcup_{i=1}^{\infty} A_i$ and $\bigcap_{i=1}^{\infty} A_i$. Consider the sample space $\Omega = \{1, 2, 3\}$. Following the definition of a sigma field, $\mathscr{F} = \{\emptyset, \Omega, \{1\}, \{2, 3\}\}$ is a sigma field while $\mathscr{G} = \{\emptyset, \Omega\{2\}\}$ is not. Rather, the correct sigma field of $\mathscr{G}$ is $\sigma(\mathscr{G}) = \{\emptyset, \Omega, \{2\}, \{1, 3\}\}$. The notation $\sigma(\mathscr{U})$ is used to denote the smallest sigma field containing $\mathscr{U}$, where $\mathscr{U}$ is a collection of subsets of Ω. In general, such a sigma field can be constructed by,

$$\sigma(\mathscr{U}) = \bigcap_{\mathscr{A}} \{\mathscr{U} \subset \mathscr{A} : \mathscr{A} \text{ is a sigma field}\} \tag{1.2}$$

A *Borel sigma algebra* is $\mathscr{B} = \sigma(\mathscr{U})$ where $\mathscr{U}$ consists of all the open sets in $\mathbb{R}^N$.

Combining the ideas described above, a *probability space* $(\Omega, \mathscr{F}, P)$ consists of a sample space Ω, a sigma field $\mathscr{F}$ of subsets of Ω, and a probability function P on $(\Omega, \mathscr{F})$. The probability function must satisfy the three axioms of probability, which are given as:

1. $P(A) \geq 0$
2. $P(\Omega) = 1$
3. $P(A \cup B) = P(A) + P(B)$ if $A \cap B = \emptyset$

An example will help make some of these abstract concepts more concrete. Consider the experiment of tossing a fair coin. The sample space is $\Omega = \{H, T\}$ and the sigma field of events is $\mathscr{F} = \{\{H\}, \{T\}, \Omega, \emptyset\}$. Probabilities of events in $\mathscr{F}$ are $P(H) = P(T) = 1/2$, $P(\Omega) = 1$ and $P(\emptyset) = 0$.

At this point, enough background has been given to describe a *random variable* in general terms. Uncertainty quantification pioneer Gianluca Iaccarino writes, "Random variables are the building blocks for studying uncertainties in a probabilistic framework" [30]. In the simplest terms, a random variable takes events and assigns them a real number. Let X be a random variable. Then X takes an event ω from the event space Ω and maps it to a number on the real line $X(\omega) : \Omega \to \mathbb{R}$. Under such a mapping a whole region $A_B \in \Omega$ gets mapped to an interval B on the real line. A more formal definition of a random variable can be made using the language of set theory. Let $(\Omega, \mathscr{F}, P)$ be a probability space. A mapping $X : \Omega \to \mathbb{R}^N$ measurable with respect to $\mathscr{F}$ is a random variable. In other words, for any open set A in $\mathbb{R}^N$, $X^{-1}(A) \in \mathscr{F}$ is a random variable.

As an example, consider the event space $\Omega = \{1, 2, 3\}$ and the sigma field $\mathscr{F} = \{\emptyset, \Omega, \{1\}, \{2, 3\}\}$. Then if we define $Y(1) = 1$, $Y(2) = 0$, and $Y(3) = -1$ then Y is not a random variable because $\{3\} \notin \mathscr{F}$. Now, if we define $Z(1) = 1$, and $Z(2) = Z(3) = 0$ then Z is a random variable because $\{1\}$ and $\{2, 3\}$ are both in $\mathscr{F}$. This example serves to demonstrate the interconnectedness between sigma fields and event spaces.

The purpose of the preceding discussion was to build a sufficient framework to be able to state the Doob-Dynkin lemma. Let $X : \Omega \to \mathbb{R}^N$ be a random variable and let $\mathscr{B}$ be the Borel sigma algebra. The sigma algebra generated by X is $\sigma(X) = \left\{X^{-1}(F) : F \in \mathscr{B}\right\}$. The Doob-Dynkin lemma describes the relationship between a random variable and the sigma field it generates. Let $X, Y : \Omega \to \mathbb{R}^N$ be two functions. Then Y is $\sigma(X)$ measurable if and only if there exists a Borel measurable function $g : \mathbb{R}^N \to \mathbb{R}^N$ (for any $A \in \mathscr{B}, g^{-1}(A) \in \mathscr{B}$) such that $Y = g(X)$. To say that Y is "$\sigma(X)$ measurable" means that if X is known then Y is known as well [46]. When a PDE is transformed into a SPDE by treating the parameters

as random variables it is appropriate to question whether the solution of the SPDE can be described in terms of the same random variables [41]. The Doob-Dynkin lemma answers this question with a resounding yes.

1.2.2 Application to Engineering Systems

In this section, the theory of SPDEs is applied to the types of problems that typically arise in nuclear engineering. Much of the notation used in the proceeding discussion is borrowed from [58]. First, define the physical domain as $\mathscr{D} \subset \mathbb{R}^d$ where d can be 1, 2, or 3 depending on the number of spatial dimensions being considered. The boundary of the domain is designated as $\partial\mathscr{D}$. Any coordinate living in the spatial domain can be described by some vector $\mathbf{x} = (x_1, ..., x_d)$. The most general mathematical systems that are of interest can be written as,

$$\mathscr{L}(\mathbf{x}, \omega; u) = f(\mathbf{x}, \omega) \qquad \mathbf{x} \in \mathscr{D} \tag{1.3}$$

$$\mathscr{B}(\mathbf{x}; u) = g(\mathbf{x}) \qquad \mathbf{x} \in \partial\mathscr{D}. \tag{1.4}$$

Ultimately, $u : \Omega \times \mathscr{D} \to \mathbb{R}$ is sought after since u is the solution to 1.3 and 1.4, where $\mathscr{L}$ is a linear/non-linear differential operator, $\mathscr{B}$ is a boundary operator, and f and g are driving terms. The system in 1.3 and 1.4 is defined over a complete probability space $(\Omega, \mathscr{F}, P)$ with $\omega \in \Omega$, as defined previously. Of course, 1.3 and 1.4 must be well-posed in the sense of Hadamard [3]. In Hadamard's definition, well-posed mathematical models of physical phenomena satisfy three conditions:

1. Existence of a solution
2. Uniqueness of the solution
3. The solution is not sensitive to small perturbations in initial conditions

Generally, well-posed problems can be solved using stable computer algorithms. However, it is important not to confuse posedness with conditioning as the two describe very different things. Problems that are typically not well-posed, such as inverse problems, can be formulated as well-posed problems through regularization.

The problem in 1.3 and 1.4 is continuous and as such, will not have an analytic solution for practical problems in engineering applications. An infinite number of random variables are needed to fully describe the stochastic process. Since modeling such a process on a computer is impossible, the infinite-dimensional probability space must be reduced to a finite-dimensional space. The procedure to do this is referred to as the "finite-dimensional

noise assumption". The Karhunen-Loeve expansion of the stochastic space achieves this reduction in dimensionality with the benefit of being able to fully model the full stochastic space if desired [58].

Applying the Karhunen-Loeve expansion to 1.3, the random inputs can be characterized by a set of N random variables as,

$$\mathscr{L}(\mathbf{x}, Y_1(\omega), ..., Y_N(\omega); u) = f(\mathbf{x}, Y_1(\omega), ..., Y_N(\omega)) \tag{1.5}$$

where $\{Y_i(\omega)\}_{i=1}^N$ are uncorrelated random variables. By the Doob-Dynkin lemma, the solution of 1.3 and 1.4 can be expressed in terms of the same random variables $\{Y_i(\omega)\}_{i=1}^N$. Hence, the solution to the SPDE can be written as $u(\mathbf{x}, \omega) = u(\mathbf{x}, Y_1(\omega), ..., Y_N(\omega))$. Equations 1.3 and 1.4 with a discrete stochastic space can be restated as,

$$\mathscr{L}(\mathbf{x}, \mathbf{Y}; u) = f(\mathbf{x}, \mathbf{Y}) \qquad (\mathbf{x}, \mathbf{Y}) \in D \times \Gamma \tag{1.6}$$

$$\mathscr{B}(\mathbf{x}, \mathbf{Y}; u) = g(\mathbf{x}, \mathbf{Y}) \qquad (\mathbf{x}, \mathbf{Y}) \in \partial D \times \Gamma \tag{1.7}$$

where Γ_i is the image of the independent random variables $Y_i(\omega)$. Without loss of generality Γ_i can be restricted to $[0,1]$ for $i = 1, ..., N$. Consequently, the bounded stochastic space, or support, is an N-hypercube $\Gamma = [0,1]^N$. No limits have really been imposed on the stochastic space since any bounded region can be mapped to the unit hypercube. In 1.6 and 1.7 what remains is a set of independent, deterministic equations in space that can be solved using any deterministic discretization technique. The stochastic problem has essentially been decoupled from the spatial problem.

1.3 Uncertainties in Nuclear Data

1.3.1 Cross Section Uncertainty Overview

While the methods described in this thesis are applicable to a plethora of engineering applications, the target application here concerns the simulation of nuclear reactors. A main component of any reactor analysis is a description of the neutronics, the physical processes behind neutron transport inside a reactor. When studying uncertainty quantification and sensitivity analysis of the neutronics in some reactor system, the primary player has been shown to be uncertainty in cross section data [1] [33]. Cross section uncertainties for various reactions, energies, and nuclides are accumulated during their experimental determination. Many of the cross sections exhibit correlations among themselves that must be taken into account. A problem arises when one becomes interested in performing uncertainty

and sensitivity analysis on a core simulator since the simulators use processed cross section data. The experimental cross section uncertainties and covariances must be carefully propagated down through the standard cross section processing regime.

Until recently, the primary approach for cross section uncertainty propagation involved the application of first-order perturbation theory. The perturbation theory approach is described in detail in [53]. Basically, for neutronics uncertainty analysis this approach entails the solution of an adjoint transport equation for each response of interest, allowing for the efficient retrieval of sensitivity coefficients for all input data. The sensitivity coefficients can then be used to obtain response uncertainties by being operated on by the inputs' covariance matrix. However, the linear approximations in perturbation theory and generalized perturbation theory may fail in certain scenarios. In particular, if the ratio of neutron loss due to absorption is high, such as when a control rod is rapidly inserted, second order effects may become substantial [53]. In addition, while perturbation theory may be computationally efficient for problems where only a handful of responses are of interest, problems with many responses may be burdensome due to the need to solve the generalized adjoint transport equation for each response. Not to mention, implementation of the perturbation theory approach is intrusive to engineering codes which makes uncertainty quantification of coupled, multiphysics code systems infeasible.

With the recent increase in accessibility to parallel computing environments stochastic sampling methods have become popular since they do not apply any kind of approximations to the physics at hand. Consequently, for cross section uncertainty propagation sampling methods have also been adopted to replace perturbation theory. A description of the process for propagating experimental uncertainties in cross section data to few group cross sections is described in this section. The statistical sampling framework for cross section data is extremely flexible since uncertainties can be calculated for any few group parameters. The same cannot be said of perturbation theory, which must formulate responses as ratios of reaction rates. Consequently, uncertainties for few group transport cross sections and assembly discontinuity factors are difficult to obtain using generalized perturbation theory.

1.3.2 Sampling Method

The method for producing stochastically sampled few-group cross sections will be described. Although the method described is quite general, to provide clarity it will be described in the context of the Standardized Computer Analyses for Licensing Evaluation (SCALE) code [7]. Specifically, SCALE's Evaluated Nuclear Data File (ENDF) li-

braries and cross section processing utilities will be detailed. In the ENDF libraries the multigroup cross sections are assumed to be Gaussian and consequently, they can be fully characterized by their means and covariances. The SCALE 44-group ENDF/B-VII covariance matrix contains generic multigroup covariance data. For a problem where m nuclide-reaction combinations are of interest the pertinent covariance matrix is expanded to a size of $[m \cdot 44] \times [m \cdot 44]$. The Gaussian assumption imposed on the cross section values implies the cross sections can take on negative values. Since cross sections physically cannot take on negative values their distributions are truncated [37].

The first step towards obtaining perturbed few-group cross sections is to sample the generic multigroup covariance library. The covariance data schema in SCALE is given as relative values of infinitely dilute cross sections [55]. Denote the 1D energy dependent, pointwise cross section for reaction x as $\sigma_x(E)$. The infinitely dilute cross section in energy group g can then be calculated as,

$$\sigma_{x,g}(\infty) = \frac{\langle \sigma_x(E) \rangle}{\Delta u_g} \tag{1.8}$$

where the bracket notation indicates a lethargy inner product over the energy interval covered by group g. Consequently, when the multigroup covariance matrix in SCALE is sampled the resulting perturbation $\sigma'_{x,g}$ to the infinitely dilute cross sections can be expressed in terms of a perturbation factor $Q_{x,g}$,

$$\begin{aligned} \sigma'_{x,g}(\infty) &= \left(1 + \frac{\Delta\sigma_{x,g}(\infty)}{\sigma_{x,g}(\infty)}\right) \sigma_{x,g}(\infty) \\ &= Q_{x,g}\sigma_{x,g}(\infty). \end{aligned} \tag{1.9}$$

The perturbations in Eq. 1.9 will provide generic multigroup cross section values to propagate through a transport solver, which can then yield perturbed few-group cross section values. However, to make the perturbed cross sections problem specific they must undergo adjustments due to resonance self shielding. For this purpose, perturbed pointwise cross sections and perturbed Bondarenko self-shielding factors are required. The pointwise, or continuous energy, cross sections are needed to perform 1D transport calculations in the resolved resonance range while the Bondarenko factors are applicable in the unresolved energy range. Since the pointwise cross sections, Bondarenko factors, and generic infinitely dilute multigroup cross section are related algebraically it is necessary to perturb each in terms of the factor $Q_{x,g}$.

In [55] the authors show that, given a perturbation factor $Q_{x,g}$, the appropriate pointwise

cross sections perturbation can be obtained by,

$$\sigma'_x(E) = Q_{x,g}\sigma_x(E) \qquad E \in g. \tag{1.10}$$

From Eq. 1.10 it is clear that the pointwise cross section data gets perturbed uniformly in a given energy group g, which is a valid approximation if the energy width is small. The authors in [55] note that although this approximation leads to discontinuities at the energy group boundaries, it does not impact the resulting multigroup data significantly. No significant impact is expected because the multigroup data is averaged using fluxes and cross sections from the same energy bin.

At this point, infinitely dilute multigroup cross sections and pointwise cross sections can be consistently perturbed using the SCALE ENDF covariance library. To proceed with a transport calculation using perturbed parameters, perturbed Bondarenko self-shielding factors $f'_{x,g}(\sigma_0)$ are also needed. The Bondarenko factors are expressed in terms of the background cross section σ_0, pointwise cross sections, and infinitely dilute cross sections as,

$$f_{x,g}(\sigma_0) = \frac{1}{\sigma_{x,g}(\infty)} \Big\langle \frac{\sigma_x(E)}{\sigma_t(E)+\sigma_0} \Big\rangle \Big/ \Big\langle \frac{1}{\sigma_t(E)+\sigma_0} \Big\rangle. \tag{1.11}$$

Substituting Eqs. 1.9 and 1.10 into Eq. 1.11, the perturbed Bondarenko factor is obtained,

$$f'_{x,g}(\sigma_0) = \frac{1}{Q_{x,g}\sigma_{x,g}(\infty)} \Big\langle \frac{Q_{x,g}\sigma_x(E)}{Q_{t,g}\sigma_t(E)+\sigma_0} \Big\rangle \Big/ \Big\langle \frac{1}{Q_{t,g}\sigma_t(E)+\sigma_0} \Big\rangle. \tag{1.12}$$

The authors in [55] show that Eq. 1.12 can be evaluated by simply evaluating the unperturbed Bondarenko equation in Eq. 1.11 at a perturbed background cross section $\sigma'_0 = \sigma_0/Q_{t,g}$. Note that only those cross sections whose uncertainties are specified in the SCALE covariance library can be processed and propagated through transport calculations. Since covariance data for 2D scattering distributions is not available in the SCALE ENDF/B-VII covariance library, their uncertainty affects cannot be quantified in any analyses [55].

1.3.3 Cross Section Sampling in SCALE

The method described in section 1.3.2 for producing perturbed cross sections will be further described in the context of the modules in SCALE. The first step is to produce perturbation factors using the module XSUSA by sampling the SCALE ENDF/B-VII covariance library. If a total of N_1 output files of transport solver are desired then N_1 sets of perturbation factors are to be obtained. Using the perturbation factors, the SCALE module CLAROL+ yields perturbed, infinitely dilute, multigroup cross sections by essentially applying Eq.

1.9. The resulting cross sections are then passed to the module CRAWDAD+, which outputs perturbed, continuous energy cross sections. To make the multigroup cross sections problem specific they are passed to the BONAMI module, which adjusts the cross sections to account for self-shielding effects in the unresolved energy region using the Bondarenko shielding factor method. Perturbed Bondarenko factors are used in BONAMI, as output from CLAROL+ upon application of Eq. 1.12.

At this point the cross sections still need to be processed for self-shielding effects in the resolved energy region. The SCALE modules CENTRM/PMC are responsible for folding in these effects into the multigroup cross sections. CENTRM solves the neutron slowing down equation on an ultra fine spectra on the order of $\mathcal{O}(10^4)$ energy points. For the flux a linear interpolation scheme is used between energy points to produce a continuous energy solution over the entire energy range [54]. The CENTRM module incorporates actual composition, temperature, and environment dependent effects into the resonance shielded cross sections. PMC accepts the high resolution flux spectra output by CENTRM and averages pointwise nuclear data into multigroup cross sections, which are now tailored to solve the specific problem of interest.

Finally, the problem specific multigroup cross sections output by CENTRM/PMC are sent to a lattice transport solver, which in this case is the SCALE module NEWT. In general, NEWT can be replaced by any transport solver. However, for the purposes of producing few group cross sections a lattice transport solver will generate the multigroup flux distribution for some heterogeneous configuration, which is then used to generate homogenized few group cross sections and intra-assembly flux shapes. A script to extract desirable output quantities from the transport output, such as few group cross sections and kinetics parameters, is needed. Such a script is executed after each of N_1 calls to NEWT. Each call extracts a set of perturbed, few group cross sections that are ultimately propagated through a core simulator. The SAMPLER sequence in SCALE automates the process of producing perturbed cross section sets [55].

With the availability of N_1 perturbed few group cross section sets, each set containing all the nuclear data required by a core simulator, the sets can be directly propagated through the core simulator. The desired results from each simulation can then be gathered and statistically analyzed in what is referred to as the 'one-step' method. However, in what is referred to as the 'two-step' method, the N_1 perturbed few group cross section sets can be used to create a few group covariance matrix [60]. The few group covariance matrix is then sampled and each sample is propagated through the core simulator. Both the 'one-step' and 'two-step' methods have been shown to produce consistent results [60]. However, the 'two-step' method has the advantage of breaking the limitation on the number of samples

that can be propagated through the core simulator. In the 'one-step' method each core simulation requires a corresponding transport solution. Transport solutions are relatively expensive to compute when compared to core simulations. A flow diagram of the 'two-step' method is displayed in Figure 1.1. For the 'one-step' method $N_1 = N_2$ whereas for the 'two-step' method $N_2 >> N_1$, allowing for the acquisition of better statistics.

Figure 1.1: Flow diagram of 'two-step' method for core simulators.

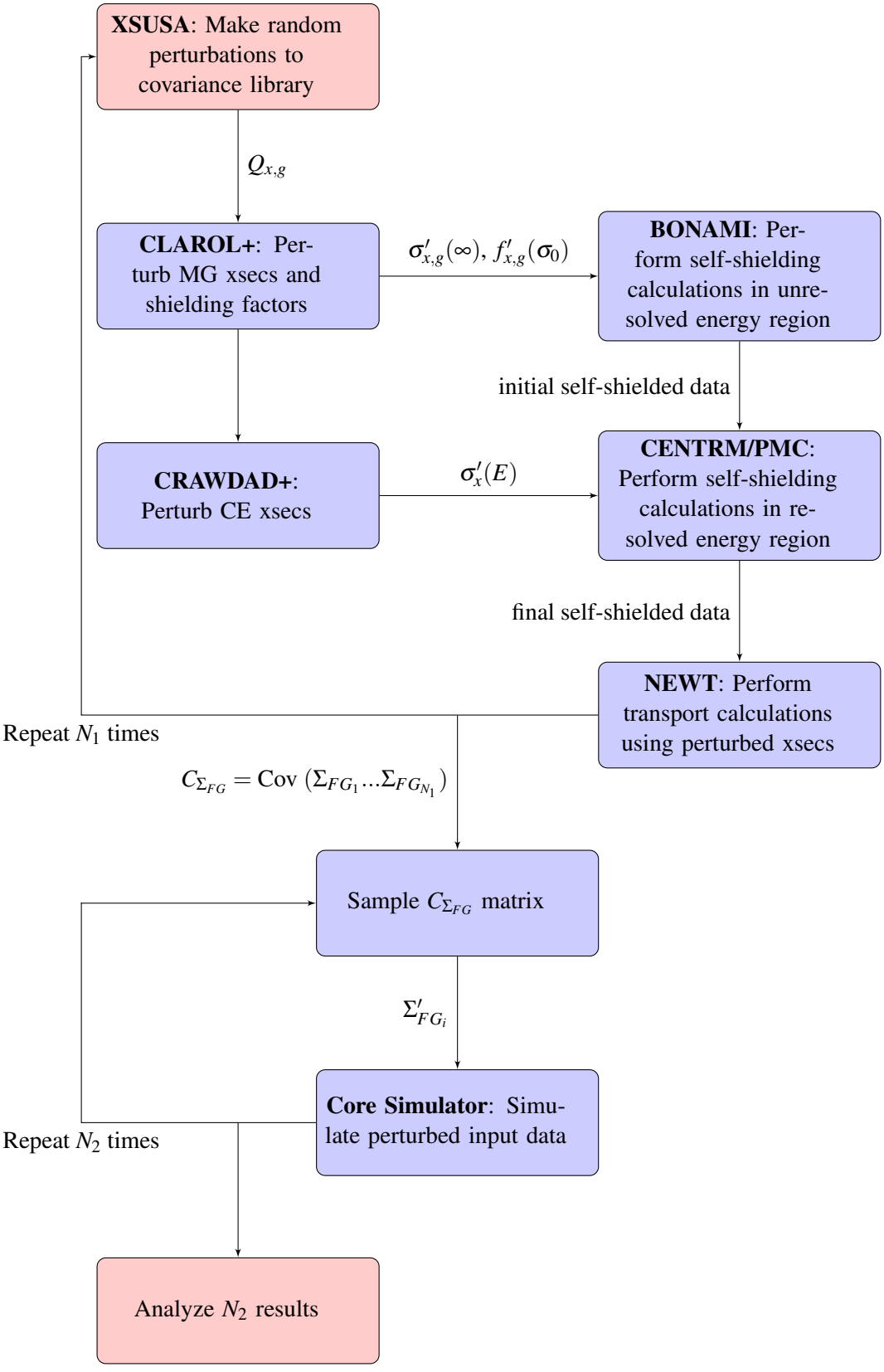

CHAPTER 2

Reduced Order Models for Computer Codes

Often an engineering team seeks to perform optimization and calibration routines on a set of computer codes which may require several hours, if not days, to complete a single simulation. Given the limited computational budget available to such teams a surrogate model is typically sought for the computational codes. The use of a surrogate model for an expensive computer code effectively exchanges predictive accuracy for simulation execution time. Unfortunately, to construct a surrogate model the expensive computer code must still be executed a certain number of times, although still significantly less times than required to conduct an optimization study. At this point there are two directions that can be taken to construct the surrogate model. If a computational budget is limited to say, N evaluations of the objective function then it is necessary to somehow optimize the set of input points at which the objective computer code is evaluated. Sampling plan optimization strategies are described in section 2.1, while surrogates based on the resulting sampling plan, namely Kriging, is described in section 2.2. If there is more flexibility in the computational budget then collocation-based surrogates should be considered since they offer the benefits of built-in convergence metrics.

Computer codes that model physical phenomena typically accept an input file whose purpose is to describe specific conditions in the universe being modeled by the code. The code is executed and the affects of the conditions on some dependent quantities are output. From this perspective computer codes can be viewed and treated in much the same way functions mathematicians deal with are treated. Like matrices, functions with certain properties can undergo various decompositions that offer insight into their structure. The purpose of section 2.3 is to describe a technique for decomposing functions into orthogonal components, with the ultimate intention of applying the technique to computer codes. It is hoped that the decomposition of the computer code in terms of its inputs reveals which inputs play the most active roles in the underlying physics. Keeping only the most active dimensions in the decomposition, a reduced order model is effectively built. However, the function decomposition technique described in section 2.3 describes only half the story.

To create a reduced order model of a computer code that can be efficiently evaluated at any state point in the original parameter space an efficient, multidimensional, interpolation scheme is needed. Such a scheme is discussed in section 2.4. The coupling between interpolation and function decomposition that creates a usable reduced order model is then described in section 2.5.

2.1 Optimized Sampling Plans

The following section is concerned with the problem of identifying an optimal set of points at which to build a surrogate model for an expensive computer code when only N evaluations can be afforded. All surrogate models are built around a set of points at which the objective computer code is actually evaluated. Intuitively, the surrogate accuracy is expected to decrease as one moves further away from such points. Consequently, it is important to spread N points as uniformly as possible across the design space.

2.1.1 Morris Algorithm

Expensive computer codes generally have many input parameters because they attempt to model some phenomena on a very fine scale as accurately as possible. Of course, when writing such computer codes engineers are not aware which input parameters have the greatest impact on the outputs of interest or else only these parameters would be modeled. Contrarily, engineers typically only know that certain parameters are involved in the pertinent physics in some way but not to what extent. Due to the curse of dimensionality, the less design variables considered in the construction of a surrogate the cheaper the computational cost will be [18]. Consequently, before attempting to construct a surrogate for an expensive computer code it is worth identifying which design variables are most active. After all, if a design variable has a trivial effect on some output of interest then its presence in the surrogate should be minimized, for this is the very purpose of a surrogate model. One method for weeding out unimportant design variables is described by Morris [44], which is summarized in algorithm 1.

The premise of Morris' algorithm is that if the derivative of some output parameter with respect to a design variable changes significantly throughout the design space then the variable is important. If the output parameter does not change with respect to the design variable then the variable can safely be ignored. To this end, the metric in Eq. 2.1 is introduced by Morris to estimate the so-called elementary effect $d_i(\mathbf{x})$ of design variable

x_i.

$$d_i(\mathbf{x}) = \frac{f(x_1, x_2, ..., x_{i-1}, x_i + \Delta, x_{i+1}, ..., x_k) - f(\mathbf{x})}{\Delta} \tag{2.1}$$

In Eq. 2.1, Δ is a step-length size for the perturbation. For convenience all variables x_i are normalized to unit length and divided into p segments such that $x_i \in \{0, 1/(p-1), 2/(p-1), ..., 1\}$. Choosing a set of $\mathbf{x}$ carefully, it is possible to calculate an elementary effect for each of k design variables using only $k+1$ function evaluations. Indeed, as described in [44], a $[k+1] \times [k]$ random orientation matrix B^* can be constructed using the equation,

$$\mathbf{B}^* = \left(\mathbf{1}_{k+1,1}\mathbf{x}^* + \frac{\Delta}{2}\left[\left(2\mathbf{B} - \mathbf{1}_{k+1,k}\right)\mathbf{D}^* + \mathbf{1}_{k+1,k} \right] \right) \mathbf{P}^*. \tag{2.2}$$

In Eq. 2.2, $\mathbf{1}$ is a matrix of ones with size specified by its subscript and $\mathbf{B}$ is a $[k+1] \times [k]$ matrix of zeros and ones with the characteristic that for each column there exists a pair of rows differing in only their i^{th} entry for $i \in \{1, 2, ..., k\}$. Also, $\mathbf{D}^*$ is a $[k] \times [k]$ diagonal matrix with ones of differing parity uniformly spread, $\mathbf{P}^*$ is a $[k] \times [k]$ random permutation matrix, and $\mathbf{x}^*$ is a random point chosen in the p-level design space. When the rows of $\mathbf{B}^*$ are evaluated by the objective function and substituted into Eq. 2.1 an elementary effect is calculated for each design variable.

The more elementary effects that can be calculated for each design variable, the better the estimate as to the effect of each design variable on the objective function. Consequently, r random orientation matrices are typically created to obtain a total of r elementary effects for each design variable. Taking the mean and standard deviation of each variable's r effects can yield insight into the most important variables. Plotting the mean and standard deviation of each variable's effects on a scatter plot, variables that have a negligible effect on the objective function will cluster around the origin. Large fluctuations in standard deviation are indicative of nonlinear and interactive effects [44].

2.1.2 Latin Hypercube Sampling

One of the major problems with random sampling occurs when a relatively limited sample size is utilized. In this case, subsets of the sample space with high consequence but low probability are likely to be missed [26]. In addition, the proximity of sampled values caused by random sampling is inefficient, which often causes slow convergence. In order to resolve such issues Latin Hypercube Sampling (LHS) was conjured. The basis of LHS rests upon dividing the normalized space of each design variable into n equally sized bins if n samples are required. As a result, when the n samples are taken it is guaranteed that the entire spectrum of each design variable's space has been visited. Algorithmically an n sample

Algorithm 1 Uses Morris' Algorithm to determine which of a function's design variables induce the most significant effects and interactions.

Initialize zeros matrix d_{stats} of size $[r] \times [k]$
for $i = 1 : r$ **do**
    $X \rightarrow$ Create random orientation matrix ▷ Eq. 2.2
    $f_{base} = f(X[0,:])$
    for $j = 1 : k$ **do**
        $f_{new} = f(X[k,:])$
        $l \rightarrow$ Find index of effect being perturbed
        $d_{effect} \rightarrow$ Calculate elementary effect ▷ Eq. 2.1
        $d_{stats}[i,l] = d_{effect}$
        $f_{base} := f_{new}$
    end for
end for
Return mean and standard deviation of d_{stats}

Latin hypercube in k dimensions can be easily calculated, as described in algorithm 2.

Algorithm 2 Creates a random Latin hypercube consisting of n samples in k dimensions.

Initialize zeros matrix X of size $[n] \times [k]$
for $i = 1 : k$ **do**
    $p \rightarrow$ Create random permutation of the set $\{1, 2, ..., n\}$
    $X[:,i] := p[:]$
end for
Map each entry of X into hypercube
Return X

Each row of the output from algorithm 2 is a sample point normalized to a hypercube. As mentioned previously, when sampling a design space it is important to take sample points uniformly. While LHS increases the likelihood of obtaining such a uniform sampling space at random it is actually possible to obtain an optimized sampling space based on the maximin metric [18].

The maximin metric describe by Morris and Mitchell [45] makes use of two notions in an attempt to quantify the uniformity, or 'space-fillingness', of a set of sampling points. In order to describe the notions for each sampling plan it is useful to gather $\{d_1, d_2, ..., d_m\}$ and $\{J_1, J_2, ..., J_m\}$, the unique distances between all points in the plan sorted in ascending order and the number of occurrences of each distance, respectively. In words, the Morris and Mitchell criteria states that an optimized sampling plan will minimize all J_i while maximizing the corresponding d_i. More formally, Morris and Mitchell define the maximin sampling plan as one which maximizes d_1, and among plans for which this is true, minimizes J_1, among plans for which this is true, maximizes d_2, and so on [18]. The previous

definition can be restated into pseudo-equivalent minimization problem by introducing the parameter $\Phi_q(\mathbf{X})$,

$$\Phi_q(\mathbf{X}) = \left(\sum_{j=1}^{m} J_j d_j^{-q} \right)^{1/q} \tag{2.3}$$

where $\mathbf{X}$ is a sampling plan and q is a control parameter inherent in the minimization problem.

The minimization of Eq. 2.3 and the Morris and Mitchell definition of the maximin sampling plan are generally used in unison to obtain a locally optimal sampling plan since finding the globally optimal plan is computationally infeasible. In this approach a random sampling plan $\mathbf{X}_0$ is initially generated using algorithm 2. Using a range of q values, usually from one to one-hundred, an optimal latin hypercube plan is found for each value based on the initial sampling plan $\mathbf{X}_0$. To obtain an optimized plan for each q algorithms such as simulated annealing [36] and evolutionary operation [8] can be used. These algorithms work to minimize Eq. 2.3 by comparing an initial sampling plan to perturbed versions, which are obtained by switching pairs of column entries in the output of algorithm 2. Once an optimized LHS plan is found for each q value, the resulting set of plans are contested directly against each other by explicit application of Morris and Mitchell's maximin definition. The sampling plan satisfying the maximin criteria is the locally optimal sampling plan to be used for proceeding surrogate model construction. Algorithm 3 summarizes the search for a locally optimal LHS plan.

Algorithm 3 Obtains a locally optimal LHS plan using the Morris-Mitchell minimax criteria.

1: Initialize sampling plan $\mathbf{X}_0$ ▷ Apply algorithm 2
2: $q = [1, 2, 5, 10, 20, 50, 100]$
3: $\mathbf{X}^{cands.} \rightarrow$ Initialize empty array for optimal $\mathbf{X}$ candidates
4: **for** q_i in q **do**
5: $\quad \mathbf{X}_{opt}(q_i) \rightarrow$ Find optimal $\mathbf{X}$ for q_i using simulated annealing ▷ Minimize Eq. 2.3
6: $\quad$ Add $\mathbf{X}_{opt}(q_i)$ to $\mathbf{X}^{cands.}$
7: **end for**
8: Apply Morris-Mitchell criterion between all $(\mathbf{X}_i^{cands.}, \mathbf{X}_j^{cands.})$ to find optimal plan

2.2 Kriging

The formulation of kriging is such that a deterministic computer code's output is assumed to be a stochastic process, enabling a statistical approach to a surrogate construction [47]. To this end, consider the sampling data $\mathbf{X} = \{\mathbf{x}^{(1)}, \mathbf{x}^{(2)}, ..., \mathbf{x}^{(n)}\}$, which may have come

from the result of an optimized sampling plan as described in section 2.1.2. At each datum $\mathbf{x}^{(k)}$ a random process $Y(\mathbf{x}^{(k)})$ induces an observation $y^{(k)}$. In kriging the random field can be described with a mean value of $\mathbf{1}\mu$, where $\mathbf{1}$ is a vector of length n, and a correlation matrix of the random field instances,

$$\Psi = \begin{pmatrix} cor[Y(\mathbf{x}^{(1)}), Y(\mathbf{x}^{(1)})] & \cdots & cor[Y(\mathbf{x}^{(1)}), Y(\mathbf{x}^{(n)})] \\ \vdots & \ddots & \vdots \\ cor[Y(\mathbf{x}^{(n)}), Y(\mathbf{x}^{(1)})] & \cdots & cor[Y(\mathbf{x}^{(n)}), Y(\mathbf{x}^{(n)})] \end{pmatrix}. \tag{2.4}$$

The correlation between two stochastic processes $Y(\mathbf{x}^{(i)})$ and $Y(\mathbf{x}^{(l)})$ is expressed as,

$$cor[Y(\mathbf{x}^{(i)}), Y(\mathbf{x}^{(l)})] = \exp\left(- \sum_{j=1}^{k} \theta_j |x_j^{(i)} - x_j^{(l)}|^{p_j} \right) \tag{2.5}$$

where θ_j and p_j are optimization parameters controlling the magnitude of correlation at each basis. Specifically the parameter p_j controls a correlation's smoothness while θ_j defines the spread.

Given the formulation of the observations occurring at $\mathbf{x}^{(k)}$ as instances of a stochastic process it is appropriate to discuss the likelihood of seeing the observed data. Of course, the likelihood is conditional on the parameters described in Eq. 2.5 as well as the mean and standard deviation of the random field. The likelihood of seeing the observed data can be written as,

$$L\left(\mathbf{Y}^{(1)}, ..., \mathbf{Y}^{(n)} | \mu, \sigma, \{\theta_1, ..., \theta_k\}, \{p_1, ..., p_k\}\right) = \frac{1}{(2\pi\sigma^2)^{n/2} |\Psi|^{1/2}} \times \cdots \times \exp\left[\frac{(\mathbf{y} - \mathbf{1}\mu)^T \Psi^{-1} (\mathbf{y} - \mathbf{1}\mu)}{2\sigma^2} \right]. \tag{2.6}$$

In order to maximize the likelihood L, that is, picking values for the mean and standard deviation that maximize the probability of seeing the observed data, the standard procedures taught in calculus can be applied to obtain the maximum likelihood estimators,

$$\hat{\mu} = \frac{\mathbf{1}^T \Psi^{-1} \mathbf{y}}{\mathbf{1}^T \Psi^{-1} \mathbf{1}} \tag{2.7}$$

$$\hat{\sigma}^2 = \frac{(\mathbf{y} - \mathbf{1}\mu)^T \Psi^{-1} (\mathbf{y} - \mathbf{1}\mu)}{n}. \tag{2.8}$$

The estimators in Eq. 2.7- 2.8 are actually estimators of the natural logarithm of the likelihood since this form is easier to work with. Substitution of Eq. 2.7- 2.8 into the natural

logarithm likelihood leads to the so called concentrated ln-likelihood function [18], given as,

$$\log(L) \approx -\frac{n}{2}\log\left(\hat{\sigma}^2\right) - \frac{1}{2}\log|\Psi|. \tag{2.9}$$

While it is relatively easy to optimize the natural logarithm likelihood with respect to μ and σ it is much more difficult to optimize Eq. 2.9 with respect to the θ and p parameters discussed earlier. Indeed, global search algorithms such as simulated annealing [36] are generally used to find optimizing θ and p parameters. Since such search algorithms require repetitive calls to the objective function, in this specific optimization problem it is important to be able to evaluate Eq. 2.9 efficiently. Quick inspection of Eqs. 2.7 - 2.9 leads to the observation that Ψ must be inverted, a common computational bottleneck for large matrices. Fortunately, being symmetric positive-definite, the matrix inversion action of Ψ can be completed efficiently by performing Cholesky decomposition followed by calls to forward and backwards substitution routines.

Once all optimizing parameters are available the goal is to utilize the parameters to build a model that makes function predictions on new points $\mathbf{x}$. Of course, the prediction should be consistent with all correlation parameters. To this end, for some new data point $\mathbf{x}$ a vector of correlations with existing points must be constructed using Eq. 2.5,

$$\psi = \begin{pmatrix} cor[Y(\mathbf{x}^{(1)}), Y(\mathbf{x})] \\ \vdots \\ cor[Y(\mathbf{x}^{(n)}), Y(\mathbf{x})] \end{pmatrix}. \tag{2.10}$$

Using Eq. 2.10 new predictions can be made at $\mathbf{x}$ using the maximum likelihood estimator,

$$\hat{y}(\mathbf{x}) = \hat{\mu} + \psi^T \Psi^{-1}\left(\mathbf{y} - \mathbf{1}\hat{\mu}\right). \tag{2.11}$$

To get some intuition for Eq. 2.11, it is worth while to consider the second term on the right-hand side as a perturbation to the mean of the stochastic process. The term $\Psi^{-1}\left(\mathbf{y} - \mathbf{1}\hat{\mu}\right)$ is a vector of coefficients of the unique linear expansion of $\left(\mathbf{y} - \mathbf{1}\hat{\mu}\right)$ in the basis columns of Ψ. From this point of view, prediction using kriging works to estimate a function value at a certain point by computing a weighted average of known function values in the vicinity of the objective points [31].

2.3 Function Decompositions

In order to reduce the dimensionality of some function there must exist a metric to determine the importance of each dimension with respect to the others. It's important to have a framework that isolates the effects of each dimension on the output of the function. The framework chosen to perform dimension reduction is formally known as high-dimensional model representation (HDMR). In statistics, the ANOVA decomposition is a special case of HDMR where the Lebesgue measure is used to perform all integrations.

2.3.1 Dimension-wise Decompositions

The dimension-wise HDMR is algorithmically similar to Gram-Schmidt for matrix orthogonalization in that orthogonal components are systemically removed to create a linearly independent basis. As in Gram-Schmidt, the essential operator in dimension-wise HDMR is the projection operator. Before introducing the projection operator of interest in this thesis, define the d-dimensional product measure to be,

$$d\mu(\mathbf{x}) = \prod_{j=1}^{d} d\mu_j(x_j) \tag{2.12}$$

where μ_j are probability measures defined over some Ω. Two functions $f, g : \Omega^d \to \mathbb{R}$ are considered orthogonal with respect to the product measure defined in 2.12 if the inner product,

$$(f,g) = \int_{\Omega^d} f(\mathbf{x}) g(\mathbf{x}) d\mu(\mathbf{x}) \tag{2.13}$$

is equal to zero. To introduce the projection operator $P_{\mathbf{u}}$, the notation used in [28] is adopted. The operator $P_{\mathbf{u}}$ projects from a d-dimensional space to a $|\mathbf{u}|$-dimensional space for some set $\mathbf{u} \subseteq \mathscr{D}$, where $\mathscr{D} = \{1, ..., d\}$ consists of the set of all coordinate indices in $\mathbf{x}$. The projection on to $\mathbf{u}$ is given as,

$$P_{\mathbf{u}} f(\mathbf{x}_{\mathbf{u}}) = \int_{\Omega^{d-|\mathbf{u}|}} f(\mathbf{x})\, d\mu_{\mathscr{D}\setminus\mathbf{u}}(\mathbf{x}) \tag{2.14}$$

where $\mathbf{x}_{\mathbf{u}}$ has length $|\mathbf{u}|$ and consists of the $\mathbf{x}$ coordinates specified in $\mathbf{u}$. Also, the notation $\mathscr{D} \setminus \mathbf{u}$ signifies all the coordinates in $\mathscr{D}$ not contained in $\mathbf{u}$. From 2.14 it is clear that the projection operator works to integrate out all coordinate indices not contained in $\mathbf{u}$ from f. For some coordinate indice sets $\mathbf{u}$ and $\mathbf{v}$, where $\mathbf{u} \neq \mathbf{v}$, the following orthogonality relation holds,

$$(f_{\mathbf{u}}, f_{\mathbf{v}}) = 0. \tag{2.15}$$

The notation $f_{\mathbf{u}}$ is used to denote the function of only the coordinate indices contained in $\mathbf{u}$. From 2.15, it follows that a function can be written in terms of its 2^d orthogonal components,

$$f(\mathbf{x}) = \sum_{\mathbf{u} \subseteq \mathscr{D}} f_{\mathbf{u}}(\mathbf{x}_{\mathbf{u}}) \tag{2.16}$$

where the component functions $f_{\mathbf{u}}$ are defined recursively as [28],

$$f_{\mathbf{u}}(\mathbf{x}_{\mathbf{u}}) = P_{\mathbf{u}} f(\mathbf{x}_{\mathbf{u}}) - \sum_{\mathbf{v} \subset \mathbf{u}} f_{\mathbf{v}}(\mathbf{x}_{\mathbf{v}}). \tag{2.17}$$

The recursive definition in 2.17 can be written explicitly as,

$$f_{\mathbf{u}}(\mathbf{x}_{\mathbf{u}}) = \sum_{\mathbf{v} \subseteq \mathbf{u}} (-1)^{|\mathbf{u}|-|\mathbf{v}|} P_{\mathbf{v}} f(\mathbf{x}_{\mathbf{v}}) \tag{2.18}$$

For most functions arising in engineering applications, especially if the function is a computer code, the decomposition in 2.16 is not possible to obtain because each component function $f_{\mathbf{u}}$ will require a high-dimensional integral to be performed. Of course, this statement assumes a Lebesgue measure in the definition of $d\mu$ in 2.12. Alternatively, if a Dirac measure is used then the computationally burdensome integral in 2.14 is reduced to a single function evaluation. In this case, the decomposition in 2.16 is referred to as an anchored-ANOVA decomposition, or CUT-HDMR [42].

2.3.2 Anchored-ANOVA Decomposition

Using the Dirac measure $\delta(\mathbf{x}-\mathbf{a})d\mathbf{x}$ to evaluate the projection operator at a fixed point $\mathbf{a} \in [0,1]^d$ in the hypercube, equation 2.14 becomes,

$$P_{\mathbf{u}} f(\mathbf{x}_{\mathbf{u}}) = f(\mathbf{x})|_{\mathbf{x}=\mathbf{a}\setminus\mathbf{x}_{\mathbf{u}}}. \tag{2.19}$$

The notation $\mathbf{a} \setminus \mathbf{x}_{\mathbf{u}}$ is the anchor point $\mathbf{a}$ except at the coordinate indices specified in $\mathbf{u}$. At the coordinate indices $\mathbf{u}$, the anchor point takes upon the corresponding values in $\mathbf{x}$. Using the Dirac measure to evaluate the projections comprising 2.16, the objective function is expressed as a linear combination of its values along lines, faces, hyperplanes,..., etc [28]. As mentioned previously, using the Dirac measure to perform the projection operations in HDMR results in enormous computational savings since high-dimensional integrals are replaced with single function evaluations.

Given the structure of anchored-ANOVA, it is not surprising to learn that there exists a close connection to multivariate Taylor series [39]. This connection provides insight into

some of the properties of the anchored-ANOVA decomposition. The multivariate Taylor series of $f(\mathbf{x})$ about a point $\bar{\mathbf{x}}$ can be written as,

$$f(\mathbf{x}) = f(\bar{\mathbf{x}}) + \sum_{i=1}^{d} \frac{\partial f(\mathbf{x})}{\partial x_i}(x_i - \bar{x}_i) + \frac{1}{2!}\sum_{i,j=1}^{d} \frac{\partial^2 f(\mathbf{x})}{\partial x_i \partial x_j}(x_i - \bar{x}_i)\left(x_j - \bar{x}_j\right) + \ldots \tag{2.20}$$

As an example, consider what happens if 2.20 is evaluated at $\mathbf{x} = \mathbf{a} \setminus x_i$,

$$f(\mathbf{x})|_{\mathbf{x}=\mathbf{a}\setminus x_i} = f(\bar{\mathbf{x}}) + \frac{\partial f(\mathbf{x})}{\partial x_i}(x_i - \bar{x}_i) + \frac{1}{2!}\frac{\partial^2 f(\mathbf{x})}{\partial x_i^2}(x_i - \bar{x}_i)^2 + \ldots \tag{2.21}$$

Since $f_i(x_i) = f(\mathbf{x})|_{\mathbf{x}=\mathbf{a}\setminus x_i} - f(\bar{\mathbf{x}})$,

$$f_i(x_i) = \frac{\partial f(\mathbf{x})}{\partial x_i}(x_i - \bar{x}_i) + \frac{1}{2!}\frac{\partial^2 f(\mathbf{x})}{\partial x_i^2}(x_i - \bar{x}_i)^2 + \ldots \tag{2.22}$$

Expression 2.22 shows that the first-order component functions in anchored-ANOVA consist of entire Taylor series expansions. Similarly, second-order component functions will consist of their respective entire Taylor series expansions and so on. Consequently, a truncated anchored-ANOVA expansion will always provide a better approximation to a function than a truncated Taylor expansion [39].

2.3.2.1 Effective Dimensions

The ultimate purpose of introducing an expansion such as anchored-ANOVA is to truncate it and use the truncated portion as an approximation to the objective function. Of course, evaluation of the truncated anchored-ANOVA expansion is expected to be much more computationally efficient than the objective function. When an anchored-ANOVA decomposition is truncated, the loss incurred becomes the components 2.17 that are not being represented. Of course, in practical construction the components not represented are calculated to contribute relatively trivially. Two notions exist for classifying the dimension of a truncated anchored-ANOVA decomposition. Both notions depend on $\hat{\sigma}(f)$, which is the sum of the absolute values of the integrals of all anchored-ANOVA terms [28]

$$\hat{\sigma}(f) = \sum_{\substack{u \subseteq \mathscr{D} \\ \mathbf{u} \neq \emptyset}} |If_{\mathbf{u}}| \approx \sum_{\substack{u \subseteq \mathscr{D} \\ \mathbf{u} \neq \emptyset}} |q_{\mathbf{u}}|. \tag{2.23}$$

The notation $I\cdot$ represents an exact integral but, in practice the integral will be evaluated using some multivariate quadrature scheme and so the exact integral's approximation is

denoted by $q_{\mathbf{u}} \approx If_{\mathbf{u}}$. For some user-defined threshold $\alpha \in [0,1]$ the truncation and superposition dimensions of a truncated anchored-ANOVA expansion can be defined. The truncation dimension attempts to quantify the importance of a certain number of dimensions d_t. Mathematically, the truncation dimension is the smallest integer d_t such that,

$$\sum_{\substack{\mathbf{u}\subseteq\{1,\ldots,d_t\}\\ \mathbf{u}\neq\emptyset}} |q_{\mathbf{u}}| \geq \alpha\hat{\sigma}(f).$$

Contrastingly, the superposition dimension attempts to quantify the order of important dimensions d_s. Mathematically, the superposition dimension is the smallest dimension d_s such that,

$$\sum_{\substack{|\mathbf{u}|\leq d_s\\ \mathbf{u}\neq\emptyset}} |q_{\mathbf{u}}| \geq \alpha\hat{\sigma}(f).$$

Both definitions for the effective definition of a truncated anchored-ANOVA expansion can be directly related to the exact integral of the objective function If. Specifically, for the truncation dimension the following relation holds [28],

$$|If - \sum_{\mathbf{u}\subseteq\{1,\ldots,d_t\}} If_{\mathbf{u}}| \leq (1-\alpha)\,\hat{\sigma}\,(f)\,. \tag{2.24}$$

Similarly, for the superposition dimension the following inequality holds,

$$|If - \sum_{|\mathbf{u}|\leq d_s} If_{\mathbf{u}}| \leq (1-\alpha)\,\hat{\sigma}\,(f)\,. \tag{2.25}$$

Inequalities 2.24 and 2.25 suggest that if all the anchored-ANOVA terms are used then the exact integral of the objective function can be reproduced. However, in general the set of effective dimensions as determined by anchored-ANOVA will not be equal to the set determined by a classic ANOVA decomposition. The choice of the anchor point $\mathbf{a}$ has a direct influence on the accuracy and truncation dimension of the anchored-ANOVA expansion [20]. In [20] the authors argue that choosing the anchor point to be the centroid of the parameter space is an excellent choice for most applications. As such, in this thesis the anchor point is always chosen to be the centroid of the working parameter space Ω^d.

2.4 Smolyak Sparse Grids

In order to create a reduced-order model for some objective function the anchored-ANOVA decomposition plays a crucial role but more is needed [21]. Recall that the primary pur-

pose for constructing a reduced-order model is to replace the presumably computationally intensive objective function with something that is trivial to evaluate. Consequently, in evaluating the anchored-ANOVA decomposition at some point $\mathbf{x}$ the projections in 2.19 must be trivial to evaluate as well. As it stands, evaluating the anchored-ANOVA decomposition for some objective function is significantly more expensive than simply evaluating the function itself. To resolve this issue, a Smolyak sparse grid interpolant is created for each projection. While creating each such interpolant incurs some initial overhead, the payoff is the desired reduced order model.

2.4.1 Motivation

To describe multivariate function interpolation based on Smolyak sparse grids it makes sense to speak in the context of quadrature since a quadrature rule consists of interpolating a function using polynomials and then integrating the polynomials exactly. For the moment consider some smooth 1D function $f(x)$. The function $f(x)$ can be approximated arbitrarily well through the summation,

$$f(x) \approx \sum_{i=1}^{P} f(x_i) C_i(x) \tag{2.26}$$

where $C_i(x)$ are cardinal functions of degree P with the property that $C_i(x_j) = \delta_{ij}$, δ_{ij} being the Kronecker δ-function [9]. By the Weierstrass approximation theorem, smooth functions can be uniformly approximated as closely as desired by polynomial functions [52]. At the collocation points, or abscissas, in 2.26 the function $f(x)$ is interpolated exactly at x_i. The function $f(x)$ is comprised of various constant, linear, quadratic, cubic,..., etc terms and so exact integration of $f(x)$ amounts to integrating its monomial constituents.

Suppose that instead of interpolating a 1D function, a multivariate function of d dimensions is to be interpolated. The naive approach to multivariate interpolation is to take a Cartesian product of 1D rules, such as in 2.26, d times. Consequently, the product grid will contain P^d points, each of which requires a unique function evaluation. Such exponential growth is coined the "curse of dimensionality" [43]. As a rule of thumb, exact integration of a monomial constituent comes at the cost of a single function evaluation [12]. Considering the space of d-dimensional, P-degree polynomials has some,

$$\binom{P+d}{d} \approx \frac{d^P}{P!} \tag{2.27}$$

dimensions, for high dimensional problems the full Cartesian product approach integrates a superfluous number of monomials. Russian mathematician Sergei Smolyak was one of

the first to realize the potential computational savings in his paper [49].

2.4.2 Algorithm Mechanics

A Smolyak sparse grid is the set of collocation points used to build an interpolant for some multivariate objective function while the Smolyak algorithm is the whole procedure of building the interpolant. To begin, the Smolyak algorithm will be stated and pertinent notation will be introduced. Since indice tracking comprises the brunt of understanding the Smolyak algorithm, it is crucial to choose a clear notation. Consequently, the notation used here closely follows that of [5].

Slightly generalizing 2.26, for the case of some smooth 1D function f, let U^i be the interpolant of f comprised of m_i collocation points.

$$U^i = \sum_{j=1}^{m_i} f\left(x_j^i\right) a_j^i \tag{2.28}$$

In 2.28, $i \in \mathbb{N}$, and $a_j^i \in C([-1,1])$ are basis functions imposing the demand that U^i exactly be able to reproduce f at the collocation points x_j^i. The notation $x_j^i \in [-1,1]$ refers to the j^{th} collocation point of m_i total points. Restricting the domain of the collocation points to $[-1,1]$ does not impose any limitations on being able to interpolate f arbitrarily well since $[-1,1]$ can always be mapped to the parameter space of f.

To generalize from 1D interpolation to multivariate interpolation 1D interpolation formulas, such as the one in 2.28, are combined using tensor products.

$$\left(U^{i_1} \otimes \cdots \otimes U^{i_d}\right)(f) = \sum_{j_1=1}^{m_{i_1}} \cdots \sum_{j_d=1}^{m_{i_d}} f\left(x_{j_1}^{i_1}, \cdots, x_{j_d}^{i_d}\right) \cdot \left(a_{j_1}^{i_1} \otimes \cdots \otimes a_{j_d}^{i_d}\right) \tag{2.29}$$

Tensor products are a mathematical convenience used to represent all combinations of some entity, in this case U^i. The scheme in 2.29 suffers from the, "curse of dimensionality" since a total of,

$$\prod_{k=1}^{d} m_{i_k} \tag{2.30}$$

function evaluations are needed to form the interpolant. The Smolyak algorithm is based on 2.29, the only difference being not all the tensor products are used. In explicit form, the Smolyak formula for approximating the left-hand side of 2.29 is given as [5],

$$A(q,d) = \sum_{q-d+1 \le |\mathbf{i}| \le q} (-1)^{q-|\mathbf{i}|} \binom{d-1}{q-|\mathbf{i}|} \left(U^{i_1} \otimes \cdots \otimes U^{i_d}\right). \tag{2.31}$$

Each entry i_k in the vector $\mathbf{i} \in \mathbb{N}^d$ contains the indice corresponding to the level of interpolation in dimension k. The more collocation points being utilized, the higher the level of interpolation since the interpolant becomes increasingly accurate. The magnitude of $\mathbf{i}$ is $|\mathbf{i}| = |i_1 + \cdots + i_d|$. Since each $i_d \geq 1$, the variable $q \geq d$. The variable q essentially keeps track of the level of interpolation of the Smolyak algorithm. As q is increased, more tensor product combinations are allowed. From 2.31 it is clear that the Smolyak algorithm is able to reduce the total number of tensor product components by limiting the entries of $\mathbf{i}$.

The Smolyak formula in 2.31 can be rewritten in several ways, all of which use the idea of the incremental interpolant Δ^i defined as,

$$\begin{aligned} U^0 &= 0 \\ \Delta^i &= U^i - U^{i-1} \end{aligned} \tag{2.32}$$

The incremental interpolant operator is simply the difference between interpolants at two successive levels. Using the notion of the incremental interpolant, the Smolyak formula can be rewritten as,

$$A(q,d) = \sum_{|\mathbf{i}| \leq q} \left(\Delta^{i_1} \otimes \cdots \otimes \Delta^{i_d} \right) \tag{2.33}$$

At first sight, 2.31 and 2.33 seem inefficient since neither exposes the recursiveness inherent in the Smolyak formula. In other words, when moving from index q to $q+1$ the work done to get to level q is not lost. Rewriting the Smolyak formula in a recursive fashion is advantageous for implementation on a computer.

$$A(q,d) = A(q-1,d) + \Delta A(q,d) \tag{2.34}$$

$$\Delta A(q,d) = \sum_{|\mathbf{i}| = q} \left(\Delta^{i_1} \otimes \cdots \otimes \Delta^{i_d} \right) \tag{2.35}$$

While the Smolyak algorithm representation in 2.34 has the advantage of being represented recursively, it does not provide any type of indicator for when the Smolyak sparse grid should be refined. Collocation points should be added to a Smolyak sparse grid until the resulting interpolant is able to reproduce the objective function to some user-defined threshold. The authors in [41] are able to rewrite 2.35 in terms of what's referred to as a hierarchical surplus,

$$\Delta A(q,d) = \sum_{|\mathbf{i}| = q} \left(f(x_{j_1}^{i_1}, ..., x_{j_d}^{i_d}) - A(q-1,d)(x_{j_1}^{i_1}, ..., x_{j_d}^{i_d}) \right) \cdot \left(a_{j_1}^{i_1} \otimes \cdots \otimes a_{j_d}^{i_d} \right) \tag{2.36}$$

which appears as the first term in the summation as the difference between the function

value at the point $(x_{j_1}^{i_1},...,x_{j_d}^{i_d})$ and the Smolyak $q-1$ level interpolant value at the same point. Level q of the Smolyak algorithm generally contains all the points comprising level $q-1$ plus some new collocation points. Consequently, the level q Smolyak interpolant is expected to exactly evaluate any collocation points born in previous levels. The summation in 2.36 is taken over all the new points in level q that have not appeared in level $q-1$ since the hierarchical surplus for these will be identically equal to zero. The hierarchical surpluses provide an indicator for how well the Smolyak algorithm is interpolating some objective function. If the hierarchical surpluses are decreasing with each successive level then the Smolyak algorithm is converging.

Following the notation in [5], let $X^i = \{x_1^i,...,x_{m_i}^i\}$ be the collocation points comprising U^i. From 2.31, the total number of collocation points in a Smolyak sparse grid can be written as,

$$H(q,d) = \bigcup_{q-d+1\leq|\mathbf{i}|\leq q} \left(X^{i_1}\times\cdots\times X^{i_d}\right). \tag{2.37}$$

2.4.3 Basis and Collocation Points

The exactness of the Smolyak algorithm is decided mainly by the choice of collocation points $x_{j_k}^{i_k}$ used to build $H(q,d)$. The basis functions $a_{j_k}^{i_k}$ work to weave the collocation points together. Gaussian quadrature is a favorite of many since with only $n+1$ collocation points, all polynomials of degree $2n+1$ or less can be integrated exactly [27]. However, collocation points derived from Gaussian quadrature schemes are not nested in that $X^i \not\subset X^{i+1}$. Nestedness in the choice of collocation points is an essential feature for reducing the computational expense of applying the Smolyak algorithm. If nested collocation points are chosen for each X^{i_k} then the Smolyak sparse grid will also be nested such that $H(q-1,d)\subset H(q,d)$ [5]. Consequently, when improving the Smolyak interpolant from level $q-1$ to level q one will only have to evaluate the objective function at the points that are unique to X^i, which are given as $X_\Delta^i = X^i \setminus X^{i-1}$ [41]. The set of new points in level q of a Smolyak sparse grid are given as,

$$\Delta H(q,d) = \bigcup_{|\mathbf{i}|=q} X_\Delta^{i_1}\times\cdots\times X_\Delta^{i_d}. \tag{2.38}$$

A viable alternative to Gaussian quadrature collocation points for the Smolyak algorithm is to use Clenshaw-Curtis collocation points, which consist of the extrema of Chebyshev polynomials. While $n+1$ Clenshaw-Curtis abscissas can only exactly integrate polynomials of degree n, they have the advantage of being nested. Accuracy is sacrificed for nestedness in the Smolyak algorithm, at least in theory. In practice it has been shown that for most functions Clenshaw-Curtis quadrature performs almost on par to Gaussian quadra-

ture [51]. In other words, the double accuracy of Gaussian quadrature is rarely realized. For some level i the Clenshaw-Curtis collocation points are given by,

$$x_j^i = \begin{cases} \cos\frac{\pi(j-1)}{m_i-1} & j = 1,...,m_i \text{ if } i > 1 \\ 0 & j = 1 \text{ if } i = 1 \end{cases} \tag{2.39}$$

In order for the level i Clenshaw-Curtis abscissas to contain the level $i-1$ abscissas, a total of 2^{i-1} new points must be added. Consequently, the total number of abscissas appearing in the level i Clenshaw-Curtis scheme is given as,

$$m_i = \begin{cases} 2^{i-1}+1 & i > 1 \\ 1 & i = 1 \end{cases} \tag{2.40}$$

Another alternative to the Gaussian and Clenshaw-Curtis abscissas is Gauss-Patterson. The Gauss-Patterson set of collocation points are nested and provide a polynomial exactness of $(3n-1)/2$ with n points, which is right in between the exactness of Clenshaw-Curtis and Gaussian sets. Obtaining the Gauss-Patterson abscissas involves a rather convoluted, iterative process and so the reader is referred to [13] to review the methodology and obtain tables of the actual points. The growth rule for Gauss-Patterson goes as $2^i - 1$, which is some factor of two greater than the growth rule for Clenshaw-Curtis. In [40], the authors conclude the Gauss-Patterson collocation points are competitive with Clenshaw-Curtis when comparing the cost and accuracy of computing quadratures using the same number of function evaluations.

To weave together the collocation points forming a Smolyak sparse grid, some type of basis function a_j^i is needed, as defined in 2.28. Although the basis functions will be applied to multi-dimensional interpolation, the Smolyak algorithm conveniently scales 1D basis functions to multiple dimensions through the use of tensor products. One basis commonly used in adaptive sparse grids is the linear hat basis function [2]. For the scheme in 2.40 the linear hat functions are given as,

$$\begin{aligned} a_1^1 &= 1 \text{ for } i = 1, \\ a_j^i &= \begin{cases} 1-(m_i-1)|x-x_j^i| & \text{if } |x-x_j^i| < 1/(m_i-1) \\ 0 & \text{else} \end{cases} \end{aligned} \tag{2.41}$$

for $i > 1$ and $j = 1,...,m_i$. While the linear hat functions have the advantage of local support they are limited to relatively slow convergence due to their lack of curvature. Offering faster

error decay are the global Lagrange characteristic polynomials,

$$a_j^i = \begin{cases} 1 & \text{if } i = 1 \\ \prod\limits_{\substack{k=1 \\ k \neq j}}^{m_i} \dfrac{x - x_k^i}{x_j^i - x_k^i} & j = 1, ..., m_i \text{ for } i > 1 \end{cases} \tag{2.42}$$

However, the Lagrange characteristic polynomials are plagued by the fact that each evaluation of 2.28 requires $\mathcal{O}(m_i^2)$ operations and often the computation is numerically unstable [6]. To remedy these concerns, the barycentric form of Lagrange characteristic polynomials is used to form a basis. The barycentric Lagrange basis is given as,

$$a_j^i = \begin{cases} 1 & \text{if } i = 1 \\ \dfrac{\frac{w_j^i}{x - x_j^i}}{\sum_{j=0}^{m_i} \frac{w_j^i}{x - x_j^i}} & j = 1, ..., m_i \text{ for } i > 1 \end{cases} \tag{2.43}$$

where w_j^i are barycentric weights defined by,

$$w_j^i = \frac{1}{\prod\limits_{k \neq j} \left(x_j^i - x_k^i\right)} \qquad j = 1, ..., m_i. \tag{2.44}$$

For special collocation sets, such as Clenshaw-Curtis in 2.39, explicit forms exist for the barycentric weights. Generally, forming the weights is an $\mathcal{O}(m_i^2)$ operation and then evaluation of an interpolant based on the barycentric Lagrange basis is only a $\mathcal{O}(m_i)$ operation [6]. With an explicit form in hand, evaluation of the barycentric Lagrange basis is significantly cheaper than the Lagrange basis. For the Clenshaw-Curtis collocation points in 2.39, the barycentric weights are given by [48],

$$w_j^i = (-1)^{j+1} \delta_j^i \qquad \delta_j^i = \begin{cases} .5 & j = 1 \text{ or } j = m_i \\ 1 & \text{else} \end{cases}. \tag{2.45}$$

From 2.43, an apparent problem exists if the barycentric basis is to be evaluated at a collocation point. As [6] explains, the problem can be circumvented by simply perturbing the value of x by an ε on the order of machine precision. In this case, the numerator and denominator in 2.43 will effectively cancel each other such that $a_j^i = 1$. The barycentric Lagrange basis is therefore numerically stable.

2.4.4 Exactness and Error Bounds

The exactness of the Smolyak algorithm is determined by the space of polynomials the algorithm is exact on. Since the 1D interpolation rules, on which the Smolyak algorithm is based on, can exactly interpolate certain polynomials it is not presumptuous to expect the Smolyak algorithm to exactly interpolate certain polynomial spaces. Using the collocation set in 2.40 and 2.39 the Smolyak interpolant $A(q,d)$ is exact on [5],

$$\sum_{|\mathbf{i}|=q} \mathbb{P}(m_{i_1}-1,1)\otimes\cdots\otimes\mathbb{P}(m_{i_d}-1,1) \tag{2.46}$$

where $\mathbb{P}(k,d)$ is the space of all polynomials in d dimensions of total degree no greater than k. From 2.46 it follows that the Smolyak interpolant for $q = d+P$ is exact for all polynomials of degree P. In other words, the effects of any monomials containing x^l for $l \leq P$ will be captured by the Smolyak algorithm. Recall from 2.27 that the degrees of freedom of $\mathbb{P}(P,d)$ goes as $d^P/P!$. Any method aiming to reproduce $\mathbb{P}$ requires at least this many function evaluations. Since the number of collocation points in a Smolyak grid for $A(d+P,d)$ goes as $2^P d^P/P!$ the dependence on dimension is said to be optimal [5]. However, the asymptotic growth of points also indicates that the Smolyak algorithm requires still excessive function evaluations to achieve polynomial exactness.

Since the Smolyak algorithm is constructed using one-dimensional interpolation formulas, which all have error bounds, it is also possible to derive error bounds for a Smolyak interpolant $A(q = d+P,d)$. While the reader is instructed to consult [5] for a detailed derivation of the error bounds, they will nevertheless be stated here. Consider some d-variable function f with continuous derivatives of order P in each variable. The error in using a Smolyak interpolant to approximate f can be given as,

$$\|f - A(d+P,d)(f)\|_\infty \leq c_{d,P} M^{-P} (\log M)^{(P+2)(d-1)+1} \tag{2.47}$$

where M is the total number of knots used by $A(d+P,d)$ and $c_{d,P}$ is a constant depending on both d and P. From 2.47, the error in the Smolyak interpolant heavily depends on the smoothness of the function being interpolated and on the total number of collocation points used to form the interpolant.

2.4.5 Computer Implementation

To implement Smolyak's algorithm on a computer equations 2.34 and 2.36 should be utilized since together they provide a recursive definition. Much of the implementation ef-

forts are concerned with indice book keeping. Although the pseudocode for Smolyak's algorithm used in this thesis is provided here, the reader is directed to [38] for more elaborate details. Efficiency of the algorithm can be increased by pre-calculating the desired abscissas as in 2.39, the number of abscissas at a given level as in 2.40, and corresponding barycentric weights as in 2.45. A data structure for quick retrieval of the desired values is also necessary. Abscissa information is constantly being reused in Smolyak's algorithm and so it is inefficient to have to recalculate values each time.

Algorithm 4 Smolyak's algorithm for creating an interpolant for a function f of d dimensions. The algorithm will exit if the maximum Smolyak level is reached or if one of the convergence criteria is met.

```
1:  Create data structure that stores indice coordinates and hierarchical surplus.
2:  for q = 0, maximum level do
3:      for (i_1, ..., i_d) in enumerations of i_1 + ... + i_d = q + d do      ▷ See Alg. 5
4:          for (j_1, ..., j_d) in enumerations of (i_1, ..., i_d) do          ▷ See Alg. 6
5:              Turn each (j_1, ..., j_d) into a knot.
6:              Categorize as either processed or unprocessed knot.
7:          end for
8:          Evaluate f(unprocessed knots).
9:          Calculate hierarchical surplus at unprocessed knots.               ▷ Eq. 2.36
10:         Archive newly processed knots.
11:     end for
12:     Check for convergence.
13: end for
```

The pseudocode for Smolyak's algorithm in algorithm 4 will now be discussed in some detail. To initialize the algorithm a data structure must be created to store all information for each index in the sparse grid. For level q of the Smolyak algorithm the summation in 2.34 is over all sets $(i_1, i_2, ..., i_d)$ such that $i_1 + i_2 + ... + i_d = q + d$. Each such set corresponds to a knot $(x_{j_{i_1}}^{i_1}, ..., x_{j_{i_d}}^{i_d})$ in the random space defined by the hypercube $[-1, 1]^d$. The knot, function value at the knot, and the corresponding hierarchical surplus should all be stored in the data structure.

The first loop in the pseudocode tells the code to keep increasing the interpolation level in the Smolyak algorithm until some maximum level is reached, which is specified by the user. The purpose of this loop is to make sure the algorithm ends eventually. Of course, other convergence criteria are in place in hope that the algorithm terminates long before the maximum level is reached. The second loop goes through all the enumerations of $(i_1, i_2, ..., i_d)$ such that $i_1 + i_2 + ... + i_d = q + d$. The algorithm for producing such enumerations is provided in algorithm 5. The third loop takes each enumeration and again enumerates over each index to obtain each component in the tensor product appearing in

the Smolyak formulation. An algorithm to execute this enumeration is provided in algorithm 6.

In the main body of the pseudocode each output from algorithm 6 is first converted to a knot $(x_{j_{i_1}}^{i_1}, ..., x_{j_{i_d}}^{i_d})$. Each potential knot must then be sorted into one of two categories. The motivation for the two categories arises from the fact that the same knot may be expressed in several ways. Since each knot corresponds to a function value and hierarchical surplus, significant computational savings can be incurred by not reevaluating the objective function at the same knots. Consequently, each potential knot is binned into either a category of knots that have already been evaluated at f or a category of unevaluated knots.

Once all components in the tensor product for a given $(i_1, i_2, ..., i_d)$ have been converted and sorted, the unevaluated knots are processed. In this step of the algorithm the previously unevaluated knots should be evaluated at f in parallel if possible since each evaluation is completely independent. The resulting functions values should then be used to compute the hierarchical surplus in 2.36 for each knot. Once the function value and hierarchical surplus is available for each new knot the results should be archived in the indice data structure.

Finally, once the second loop is complete, the level of the Smolyak interpolant has been effectively increased and it's time to check whether additional levels are required based on user-defined convergence criteria. Perhaps the best indicator of a Smolyak interpolant's convergence is the maximum hierarchical surplus calculated for all newly processed knots at the current interpolation level. The hierarchical surplus is a measure of how well the interpolant is able to match the objective function and therefore, if the hierarchical surpluses being calculated are decreasing with each level the interpolant is converging. An additional convergence criteria includes comparison of the relative change in computed mean and variance between two successive interpolation levels. For this thesis, the Smolyak algorithm is terminated only after the maximum hierarchical surplus is below a certain threshold, the relative change in interpolant mean is below a threshold, and the relative change in variance does not exceed a threshold.

2.5 Combining Decomposition and Smolyak's Algorithm

As hinted at in the beginning of chapter 2, the Smolyak algorithm combines with the anchored-ANOVA decomposition to create a reduced order model for any well behaving computer code. To see how the Smolyak algorithm fits into the functional decomposition

described in this chapter, begin by substituting 2.18 into 2.16 to get,

$$f(\mathbf{x}) = \sum_{\mathbf{u}\subseteq\mathscr{D}} \sum_{\mathbf{v}\subseteq\mathbf{u}} (-1)^{|\mathbf{u}|-|\mathbf{v}|} P_{\mathbf{v}} f(\mathbf{x}_{\mathbf{v}}). \tag{2.48}$$

Now, insert the Dirac projection operator from 2.19 into 2.48 to arrive at,

$$f(\mathbf{x}) = \sum_{\mathbf{u}\subseteq\mathscr{D}} \sum_{\mathbf{v}\subseteq\mathbf{u}} (-1)^{|\mathbf{u}|-|\mathbf{v}|} f(\mathbf{x})|_{\mathbf{x}=\mathbf{a}\setminus\mathbf{x}_{\mathbf{v}}}. \tag{2.49}$$

To create a reduced order model the set $\mathscr{D}$ is ultimately shrunk to only contain a subset of all the variables of f but this is discussed later. The important aspect of 2.49 to realize is that in order to evaluate $f(\mathbf{x})|_{\mathbf{x}=\mathbf{a}\setminus\mathbf{x}_{\mathbf{v}}}$ evaluation of the expensive computer code $f(\mathbf{x})$ is required. Consequently, the desirable property of reduced order models, that of rapid evaluation, is not achieved in 2.49. The remedy is to approximate each $f(\mathbf{x})|_{\mathbf{x}=\mathbf{a}\setminus\mathbf{x}_{\mathbf{v}}}$ using Smolyak interpolants. Substituting 2.33 into 2.49, the formulation for creating a reduced order model of f is complete.

$$f(\mathbf{x}) = \sum_{\mathbf{u}\subseteq\mathscr{D}} \sum_{\mathbf{v}\subseteq\mathbf{u}} (-1)^{|\mathbf{u}|-|\mathbf{v}|} \sum_{|\mathbf{i}|\leq q} \left(\Delta^{i_1} \otimes \cdots \otimes \Delta^{i_{|\mathbf{v}|}}\right) \tag{2.50}$$

While there is initial overhead to create an interpolant for each component in 2.49 the result is quick evaluation of the reduced order model. Details regarding the implementation and application of 2.50 will be discussed in the proceeding sections.

2.5.1 Combinatorics Routines

In order to implement 2.50 on a computer several enumeration routines need to be available. Unfortunately, these routines are not available in most numerical math libraries containing combinatorics routines. The first routine of interest solves the problem of how to enumerate all the ways d positive integers can be summed to equal another integer. In other words, what are all the sets $\{i_1,...,i_d\}$ such that $i_1+i_2+...+i_d = q$? This problem inserts itself in 2.50 in the summation index for Smolyak interpolation. As the Smolyak interpolant becomes refined from level to level—q is increased by one in each refinement—the Smolyak algorithm must newly account for all $\mathbf{i}$ such that $|\mathbf{i}| = q$. The following enumeration algorithm, a slight modification of the original algorithm found in [28], finds all the desired indice sets:

With all the index sets for some Smolyak level q available through the code segment in 5, the tensor product appearing in 2.33 can be evaluated with the aid of an additional

Algorithm 5 For positive integers d and q this code outputs all sets $\{i_1, i_2, ..., i_d\}$ such that $i_1 + i_2 + ... + i_d = q$.

$p = 0$
$m = q - d + 1$
$k = [0, 1, ..., 1]$ ▷ vector of length d
$\hat{k} = [m, m, ..., m]$ ▷ vector of length d
repeat
    $k(p) = k(p) + 1$
    if $k(p) > \hat{k}(p)$ **then**
        if p=d **then**
            All indices enumerated!
        else
            $k(p) = 1$
            $p = p + 1$
        end if
    else
        for $j = 0 : p$ **do**
            $\hat{k}(j) = \hat{k}(p) - k(p) + 1$
        end for
        $k(0) = \hat{k}(0)$
        $p = 1$
        Return valid index set k!
    end if
until $k = [0, ..., 0]$

enumeration routine. Each indice in an index set $\{i_1 + i_2 + ... + i_d\}$ corresponds to certain number of knots, which for example, is given by 2.40 for Clenshaw-Curtis. All the components in the tensor product can be given by the following enumeration algorithm, which is based on the algorithm in [28]. Input to algorithm 6 should be based on output from algorithm 5. Specifically for some index set $\{i_1, i_2, ..., i_d\}$ returned by algorithm 5, each indice should be converted to a corresponding number of knots and input to algorithm 6.

Algorithm 6 Code for enumerating all components of a tensor product. The input is a d dimensional vector m where each entry m_j corresponds to the number of knots in a collocation scheme of level i_j.

```
1:  p = 0
2:  s = [0, 1, 1, ..., 1]                          ▷ vector of length d
3:  repeat
4:      s(p) = s(p) + 1
5:      if s(p) > m(p) then
6:          if p = d − 1 then
7:              All indices enumerated!
8:          else
9:              s(p) = 1
10:             p = p + 1
11:         end if
12:     else
13:         p = 0
14:         Return valid enumeration set!
15:     end if
16: until s = m
```

2.5.2 Sampling Sparse Grid Interpolant of Correlated Variables

The reduced order model in 2.50 consists of linear combinations of Smolyak interpolants. Evaluation of the reduced order model is equivalent to finding the value at several Smolyak interpolants and summing the results. However, recall that in the Smolyak algorithm for building the interpolants described in 2.4.2 each dimension in the sparse grid is built orthogonal to the others. Implicit in this construction is the assumption that the random variables comprising the objective function are independent. In fact, in many computer codes the random variables forming the parameter space are correlated. The degree of correlation among the random variables is generally described using a covariance matrix.

With the availability of a covariance matrix for the input random variables it is possible to sample the reduced order model hundreds or thousands of times to get accurate and precise statistical moments. Evaluating a Smolyak interpolant is relatively cheap and fast

so this is not a computational problem. To produce correlated random variables from a Gaussian population the Kaiser-Dichman method can be applied [35]. Say some inputs to a computer code are normally distributed with mean μ and covariance Σ. To produce a random sample μ' from Σ one can apply,

$$\mu' = \mu + U^T \pi \tag{2.51}$$

where U^T is the lower triangular matrix arising from the Cholesky decomposition of Σ and π is a standard normal random vector.

The Cholesky decomposition of a covariance matrix $C = U^T U$ is the equivalent to taking the square root of a matrix. A Cholesky matrix transform, or left multiplication by U^T, maps uncorrelated variables into correlated variables with covariance matrix Σ. Consequently, in 2.51 μ' is normally distributed with mean μ and covariance Σ. A statistically significant number of instances of μ' should be calculated and evaluated at the reduced order model. Even though the model is built assuming independent variables this method takes into account any correlations when calculating statistical moments. When evaluating any Smolyak interpolant at a number of sampled points one must always make sure all the sampled points lay inside the bounds of the hypercube forming the sparse grid.

2.5.3 Dimension Truncation

By definition a reduced order model contains less dimensions than the original model whose reduction is intended. Consequently, a methodology for identifying important dimensions is necessary. For the purposes of this thesis, the importance of a random input variable on some objective function is determined by its contribution to the function's variance. While there are methods for exactly calculating the truncation and superposition dimensions of a function [28], these methods require the computation of all 2^d component functions in an ANOVA decomposition. For typical computer codes used in engineering this requirement is not feasible and so the effective dimensions of a function must be estimated adaptively.

To this end, construction of a reduced order model based on the anchored-ANOVA decomposition begins with calculation of the zeroth-order and all first-order components. The zeroth-order component function is simply the function evaluated at the anchor point,

$$f_{\{\emptyset\}} = f(\overline{\mathbf{x}}). \tag{2.52}$$

From the recursive definition of the anchored-ANOVA decomposition in 2.17, the i^{th} com-

ponent function is given as,

$$f_{\{i\}} = f(\mathbf{x})|_{\mathbf{x}\setminus x_i} - f_{\{\emptyset\}}. \tag{2.53}$$

The first order components solely measure the affect of the i^{th} random variable on the function output. Therefore, for each of d random variables contributing to a function's variability a sensitivity coefficient can be calculated as [42],

$$\eta_i = \frac{\int_{\Omega_i} \left[f(\mathbf{x})|_{\mathbf{x}=\bar{\mathbf{x}}\setminus x_i} - f(\mathbf{x}) \right] \rho(x_i) dx_i}{f_{\{\emptyset\}}} \tag{2.54}$$

where $\rho(x_i)$ is the probability density of x_i. If f is a function of spatial coordinates then the L_2 norm can be applied to 2.54. The greater the affect of the i^{th} random variable on the function output, the greater the sensitivity coefficient.

Once all the first order anchored-ANOVA components are calculated the sensitivity coefficients in 2.54 can be used to identify the important dimensions. To start, each η_i should be normalized by the sum of all η_i. The important dimensions can then be obtained by taking all i variables such that $\eta_i > \theta_1$. A value of $\theta_1 = .02$ has been shown to be effective for many problems [21]. At the very least, the reduced order model described here will consists of the zeroth order and all first order anchored-ANOVA components, giving it a superposition dimension of one. The variance and mean of the reduced order model with superposition dimension one should be obtained through sampling using 2.51.

To improve accuracy higher order components can be included. Higher order components should only be built using combinations of the dimensions deemed important. If all dimensions were to be included construction of a reduced order model based on the ANOVA decomposition would quickly become intractable for most engineering problems. It can be argued that if a set of random variables independently affect a function then their interactions will likely also affect the function. Say all first order components have been constructed and the important dimensions have been added to a set $\mathscr{T}$. The next step in creating a higher order model is to construct anchored-ANOVA components utilizing dimensions t such that $t \subset \mathscr{T}$ and $|t| = 2$. In total there should be $C(|\mathscr{T}|, 2)$ such components. In general, the number of p order components can be given as,

$$C(|\mathscr{T}|, p) = \frac{|\mathscr{T}|!}{(p!)(|\mathscr{T}| - p)!}. \tag{2.55}$$

To determine whether additional orders need to be included in the reduced order model, the mean of the current reduced order model should be compared to the mean of the previous order model. If the relative change in mean doesn't exceed some threshold θ_2 then the

reduced order model is considered converged. Otherwise, higher order components should be added. In this manner, a reduced order model for a computer code can be constructed adaptively. The procedure for adaptively creating a reduced order model is summarized in algorithm 7.

Algorithm 7 Adaptively creates a reduced order model for some function f of d dimensions.

Create zeroth-order component function. ▷ Eq. 2.52
for $i = 1, d$ **do**
    Construct 1D Smolyak interpolant for $P_{\{i\}} f$. ▷ Eq. 2.19
    Create first-order anchored-ANOVA component $f_{\{i\}}$. ▷ Eq. 2.53
end for
Identify important dimensions and put into set $\mathscr{T}$. ▷ Eq. 2.54
for $p = 2, d$ **do**
    for $t \subset \mathscr{T}$ s.t. $|t| = p$ **do**
        Construct p-dimensional Smolyak interpolant for $P_t f$. ▷ Eq. 2.19
        Create p-order anchored-ANOVA component f_t. ▷ Eq. 2.17
    end for
    Check for convergence of reduced order model.
end for

CHAPTER 3

Application to Simplified Reactor Systems

The methodology described in Chapter 2 will initially be applied to three relatively simple problems in reactor physics, each building on its predecessors in complexity. The purpose of the simple problems is to develop some intuition about the workings of the described reduced order model algorithm. Ultimately, the methods will be applied to solve a state of the art problem in reactor uncertainty quantification and sensitivity analysis.

3.1 Infinite Lattice Multiplication Factor

3.1.1 Problem Statement

In an infinite lattice a reactor of infinite size is considered and therefore neutrons are not capable of leaking out of the system. An infinite lattice effectively removes the effects of geometry in neutron transport and characterizes the system entirely in terms of its material properties. Since the physics of an infinite lattice are greatly simplified an analytic analysis of the system is possible. Consequently, the infinite lattice problem is ideal for an initial analysis of any new computational method.

To begin, the mathematical formulation of an infinite lattice will be described. In matrix form the two-group neutron balance equations for an infinite lattice can be written as,

$$\begin{pmatrix} \Sigma_{a_1}+\Sigma_{1\to 2} & 0 \\ -\Sigma_{12} & \Sigma_{a_2} \end{pmatrix} \begin{pmatrix} \phi_1 \\ \phi_2 \end{pmatrix} = \frac{1}{k_\infty} \begin{pmatrix} \nu\Sigma_{f_1} & \nu\Sigma_{f_2} \\ 0 & 0 \end{pmatrix} \begin{pmatrix} \phi_1 \\ \phi_2 \end{pmatrix}. \tag{3.1}$$

Solving the system in 3.1 for the infinite multiplication factor, the following analytic expression is obtained,

$$k = \frac{\Sigma_{a_2}\nu\Sigma_{f_1}+\Sigma_{1\to 2}\nu\Sigma_{f_2}}{\Sigma_{a_2}\left(\Sigma_{a_1}+\Sigma_{1\to 2}\right)}. \tag{3.2}$$

The infinite multiplication factor is a function of five material parameters. Since this thesis is concerned with the affect of uncertainties in input parameters on computer code outputs,

variations in k_∞ as a function its stochastic input variables are of interest. Assume all variation in k_∞ can be attributed to its input cross sections, whose distributions follow a multivariate Gaussian. To obtain physical homogenized, two-group cross section values a real system must first be modeled in a transport code. The UAM Benchmark is sought for this purpose [32]. Specifically, the TMI assembly is modeled using the two-step method described in [60]. A total of 300 perturbed cross section sets were produced to obtain the few-group mean and covariance data used in the proceeding analysis. The cross section data is summarized in Table 3.1.

Table 3.1: Two-group cross section data for an infinite TMI lattice.

			Correlation Coefficient Matrix				
	Mean	**Standard Dev.**	Σ_{a_1}	Σ_{a_2}	$\nu\Sigma_{f_1}$	$\nu\Sigma_{f_2}$	$\Sigma_{1\to2}$
Σ_{a_1}	1.04E-02	9.06E-05	1	0.07	-0.13	0.02	0.75
Σ_{a_2}	1.10E-01	2.31E-04	0.07	1	0.06	0.31	-0.07
$\nu\Sigma_{f_1}$	9.00E-03	4.85E-05	-0.13	0.06	1	0.33	-0.10
$\nu\Sigma_{f_2}$	1.91E-01	8.87E-04	0.02	0.31	0.33	1	0.01
$\Sigma_{1\to2}$	1.80E-02	2.18E-04	0.75	-0.07	-0.10	0.01	1

Multiple methods will be applied to obtain basic statistical and sensitivity data on the infinite multiplication factor. Of course, Monte Carlo sampling using the input cross sections' covariance matrix and applying 2.51 will provide the mean and variance of k_∞. Another approach to get at the variance of k_∞ is through the "Sandwich Equation" [34],

$$\sigma^2(k_\infty) = S^T C S \tag{3.3}$$

where C is the covariance matrix for the input data. In equation 3.3 the array S contains sensitivities of the output to the input parameters. For this problem the vector S contains,

$$S^T = \left(\frac{\partial k_\infty}{\partial \Sigma_{a_1}} \quad \frac{\partial k_\infty}{\partial \Sigma_{a_2}} \quad \frac{\partial k_\infty}{\partial \nu\Sigma_{f_1}} \quad \frac{\partial k_\infty}{\partial \nu\Sigma_{f_2}} \quad \frac{\partial k_\infty}{\partial \Sigma_{1\to2}} \right). \tag{3.4}$$

Since there exists an analytic expression for k_∞ the sensitivity vector for this problem in 3.4 is exact. As a side-check the sensitivity vector S can also be constructed using central differencing. The sensitivity of k_∞ to the i^{th} cross section Σ_i using central differencing is expressed as,

$$\left.\frac{\partial k_\infty}{\partial \Sigma_i}\right|_{\Sigma_{j\neq i}=\bar{\Sigma}_j} \approx \frac{k_\infty(\Sigma_i + \Delta\Sigma_i) - k_\infty(\Sigma_i - \Delta\Sigma_i)}{2\Delta\Sigma_i} \tag{3.5}$$

where all cross sections Σ_j, $j \neq i$, are held at their mean values. Generally a one percent perturbation $\Delta\Sigma$ is sufficient to obtain accurate sensitivities although this rule of thumb is

dependent on the smoothness of the objective function. With a variety of methods available to obtain sensitivities and statistical moments of k_∞ it is possible to thoroughly assess the potential of a reduced order model.

3.1.2 Analysis

Several elements of the methodologies described in Chapter 2 will be tested in this section and compared to results obtained using analytic and Monte Carlo approaches. For all Smolyak sparse grids constructed the hypercube domain extends to six standard deviations in each random variable. Since k_∞ is a function of only five random variables a sparse grid interpolant will be constructed without applying any function decomposition in order to demonstrate the accuracy and convergence of the method. The convergence criteria for the sparse grid interpolant is set such that the maximum hierarchical surplus at a given level is not to exceed 10^{-10}. Both Clenshaw-Curtis and Gauss-Patterson abscissas are tested.

From Fig. 3.1 the Clenshaw-Curtis and Gauss-Patterson schemes perform similarly in terms of level to level convergence. However, observe that at each interpolation level the Gauss-Patterson scheme requires significantly more nodes in exchange for a small increase in convergence speed. Both schemes converge to the threshold around level five although the Gauss-Patterson scheme requires more than twice as many function evaluations to get there than Clenshaw-Curtis. Based on the graphical determination of order of convergence [9], it is clear from 3.1 that the Smolyak interpolant for k_∞ converges geometrically.

With the Smolyak interpolation routines working as expected it's safe to apply them to an anchored-ANOVA decomposition of k_∞. To start, only the first order components will be built and analyzed. The first order components are relatively cheap to produce and often collectively produce very accurate reduced order models [42]. Afterwards, all higher order components will be added in order to show that the full anchored-ANOVA decomposition can fully reproduce the objective function. Since k_∞ is a function of only five random variables there is no point in adaptively constructing the reduced order model as described in Section 2.5.3.

As a first comparison between all the models developed for quantifying the uncertainty in k_∞ the mean and variance values of each model will be compared. With the exception of the variance obtained using the Sandwich Equation, each model's variance was obtained by propagating 1000 samples of Eq. 2.51 through the model. All samples produced for each model were seeded identically and so the same random numbers were drawn. The mean and variance results, along with 99% confidence intervals, are summarized in Table 3.2.

The five dimensional sparse grid interpolant results are entirely self consistent with the

Figure 3.1: Convergence study of a five dimensional sparse grid interpolant for the multiplication factor of an infinite TMI lattice. The boxed numbers represent the current number of knots in the sparse grid.

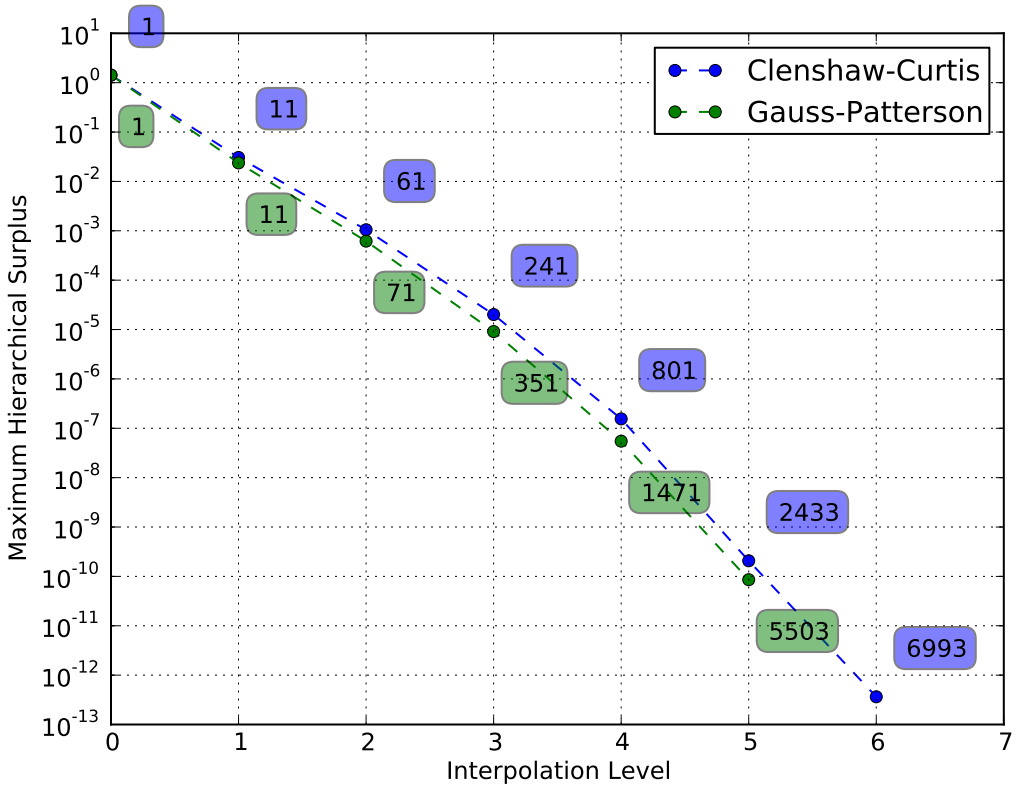

Table 3.2: Mean and variance data for the multiplication factor of an infinite TMI lattice obtained using Monte Carlo sampling. Wherever sampling was utilized the same random numbers were used.

Method	**Mean**	**99% CI**	**Standard Dev.**	**99% CI**
5D Sparse Grid CC	1.41562	(1.41512, 1.41612)	0.006168	(0.005909, 0.006544)
5D Sparse Grid GP	1.41562	(1.41512, 1.41612)	0.006168	(0.005831, 0.006544)
1D ANOVA CC	1.41560	(1.41510, 1.41610)	0.006168	(0.005831, 0.006544)
All ANOVA CC	1.41562	(1.41512, 1.41612)	0.006168	(0.005831, 0.006544)
1D ANOVA GP	1.41560	(1.41510, 1.41610)	0.006168	(0.005831, 0.006544)
All ANOVA GP	1.41562	(1.41512, 1.41612)	0.006168	(0.005831, 0.006544)
True Function	1.41562	(1.41512, 1.41612)	0.006168	(0.005831, 0.006544)
Sandwich			0.006540	

Figure 3.2: Cumulative number of knots required at each level of an anchored-ANOVA decomposition of the multiplication factor of an infinite TMI lattice. Boxes contain the calculated standard deviation at the current level.

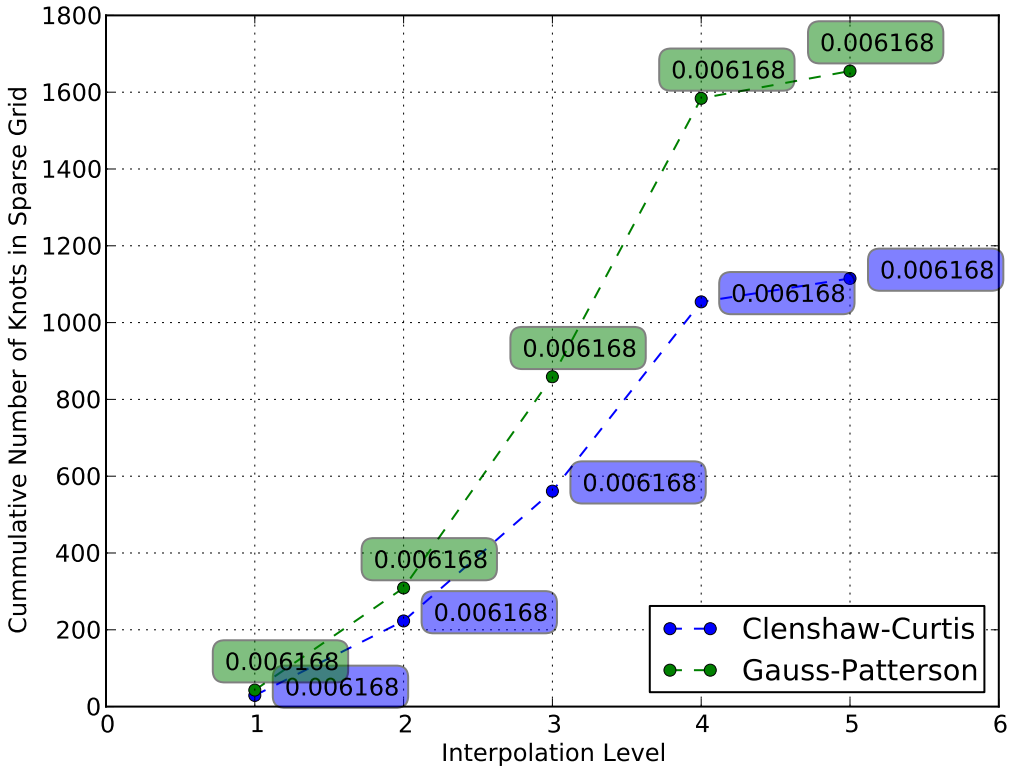

anchored-ANOVA results. Further, both of these methods produce identical results to those obtained using Monte Carlo sampling. Although the analytic variance from the Sandwich Equation is within the 99% confidence bounds of each model's results, there is a notable difference due to the fact that only 1000 samples were used to obtain each model's statistics. Increasing the number of samples decreased the difference. Note that in Table 3.2 the anchored-ANOVA the reduced order models consisting of only one dimension anchored-ANOVA components perform just as well as the full decomposition and the sparse grid interpolants over all five random variables. However, the 1D component models require only 29 function evaluations to produce, which is some ten times fewer evaluations than the 5D interpolants, and some hundred times fewer evaluations than the full decomposition. The rapid convergence of the reduced order model containing only one dimensional anchored-ANOVA components is shown in 3.2. Construction of higher order components is very expensive. Fortunately for this problem, and perhaps others, construction of only

Table 3.3: Normalized sensitivity coefficients for the multiplication factor of an infinite TMI lattice.

	Normalized Sensitivity Coefficient of k_∞				
Method	Σ_{a_1}	Σ_{a_2}	$\nu\Sigma_{f_1}$	$\nu\Sigma_{f_2}$	$\Sigma_{1\to 2}$
5D Sparse Grid CC	-.367551	-.776087	.224060	.776010	.143491
5D Sparse Grid GP	-.367551	-.776087	.224060	.776010	.143491
1D ANOVA CC	-.367556	-.776098	.224063	.776020	.143493
All ANOVA CC	-.367551	-.776087	.224060	.776010	.143491
1D ANOVA GP	-.367556	-.776098	.224063	.776020	.143493
All ANOVA GP	-.367551	-.776087	.224060	.776010	.143491
Analytic	-.367520	-.775956	.224044	.775956	.143476
Central Difference	-.367551	-.776089	.224060	.776011	.143492

one dimensional components is completely sufficient to represent the objective function.

As another performance measure of the reduced order model methodologies, each model is used to obtain normalized sensitivity coefficients for k_∞. Central differencing is applied to each model, with perturbations made to each cross section at a time while holding the other cross sections at their mean values. Perturbations are taken to be 1% of each cross section's value. Using the analytic expression for k_∞ in 3.2, the central differencing results can be compared to the true sensitivity coefficients. The results are summarized in Table 3.3. Table 3.3, sensitivity coefficients are also obtained by applying central differencing to the true function as in Eq. 3.5. As expected, all models utilizing the central differencing formula produce self consistent sensitivity coefficients. The models differ from the analytic sensitivity coefficients only in the fourth decimal place, which is expected given the $\mathcal{O}(\Delta\Sigma^2)$ convergence of the central differencing formula.

3.2 Point Kinetics/Lumped Thermal Hydraulics

3.2.1 Problem Statement

A reduced order model based on the anchored-ANOVA decomposition will be constructed in this section for a simple system of ordinary differential equations modeling a transient in a BN800 sodium fast cooled reactor. The physical model of the reactor consists of point kinetics to model the neutronics and lumped thermal hydraulics equations to describe temperature feedback. The coupled system is nonlinear and only has a time dependence. Previous research groups have utilized point kinetics and lumped thermal hydraulics equations to model basic reactor systems in [24], [23], and [29]. In this section a reduced order

model will be constructed for the maximum fuel temperature attained following a reactivity insertion as a function of the random variables exhibited in the description of the point kinetics/lumped thermal hydraulics system.

The six-group point kinetics equations modeling the neutronics of a reactor consist of a balance for reactor power $P(t)$ and a balance equation for each of the six precursor concentrations $C_k(t)$. Changes in reactor power are dependent on the precursor concentration, decays constants λ_k, delayed neutron fraction β and the mean neutron generation time Λ as detailed in,

$$\frac{dP}{dt} = \frac{\rho(T_f, T_c, t) - \beta}{\Lambda} P + \sum_{k=1}^{6} \lambda_k C_k. \tag{3.6}$$

The reactivity ρ depends on feedback from the fluids temperature models for the reactor fuel and coolant, which in turn depend on reactor power. The expression for each of the k precursor concentrations is written as,

$$\frac{dC_k}{dt} = -\lambda_k C_k + \frac{\beta_k}{\Lambda} P. \tag{3.7}$$

As for the ordinary differential equations describing the behavior of the reactor coolant system, two coupled equations suffice. For the fuel temperature T_f, the following lumped model is used,

$$M_f c_{pf} \frac{dT_f}{dt} = P + Ah(T_c - T_f) \tag{3.8}$$

where M_f is the lump fuel mass, c_{pf} is the specific heat capacity of the fuel, A is the heat transfer surface, and h is the heat transfer coefficient between the coolant and reactor fuel. Finally, the coolant temperature is described as,

$$M_c c_{pc} \left(\frac{dT_c}{dt} + v \frac{T_c - T_{in}}{L} \right) = Ah(T_f - T_c) \tag{3.9}$$

where M_c is the lump coolant mass, c_{pc} is the specific heat capacity of the coolant, L is the coolant channel length, v is the coolant flow velocity, and T_{in} is the inlet coolant temperature. The initial conditions for P, C_k, T_f, and T_c depend on the initial power in the

reactor P_0 before any kind of transient occurs and are listed in 3.10.

$$\begin{aligned} P(0) &= P_0 \\ C_k(0) &= \frac{\beta_k}{\lambda_k \Lambda} P_0 \\ T_f(0) &= T_c(0) + \frac{P_0}{Ah} \\ T_c(0) &= T_{in} + \frac{P_0 L}{M_c c_{pc} v} \end{aligned} \tag{3.10}$$

Serving as the coupling device between the lumped thermal hydraulics model and point kinetics model is the reactivity, which is proportional to the coolant temperature and the fuel temperature. Of course, any external reactivity ρ_{ex} added to the reactor is also a contributor. The time dependent reactivity is given explicitly as,

$$\rho(T_f, T_c, t) = \rho_{ex} + \alpha_d (T_f - T_f(0)) + \alpha_c (T_c - T_c(0)) \tag{3.11}$$

where α_d and α_c are the doppler and coolant coefficients of reactivity, respectively.

The equations in 3.6, 3.7, 3.9, and 3.8 are used to model the transient resulting from a half sawtooth external reactivity insertion, as shown in 3.12.

$$\rho_{ex}(t) = \begin{cases} t\rho_{max}/20 & t \leq 20 \\ 0 & t > 20 \end{cases} \tag{3.12}$$

By treating the coefficients in the point kinetics/lumped thermal hydraulics model as random variables, the objective function investigates the response surface for the maximum fuel temperature attained during transient. The reduced order methodologies will be tested against the stated problem. A depiction of the transient at the random variables' mean values, along with the external reactivity is shown in Figure 3.3. A total of twenty two random variables will be investigated for their affect on the maximum fuel temperature attained during transient. The random variables' mean values, along with their standard deviations are listed in 3.4. Note that all standard deviations are taken to be 5% of the mean value. All random variables are assumed to be independent of one another, as was assumed in [23]. A plot of the fuel temperature as a function of time due to the external reactivity profile shown in the same figure is depicted in Figure 3.4.

Figure 3.3: Transient resulting from a half sawtooth external reactivity insertion, as modeled using the mean parameter values of the point kinetics/lumped thermal hydraulics system.

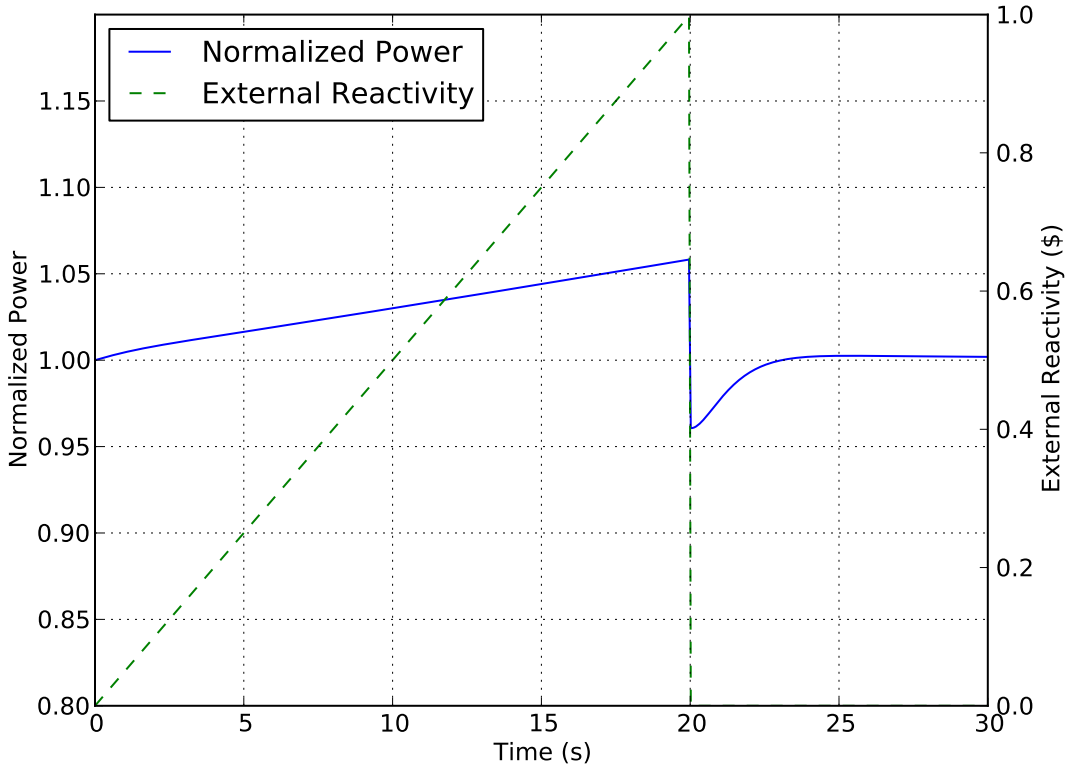

Table 3.4: Mean parameter values used in the point kinetics/lumped thermal hydraulics model for the analysis of a BN800 fast sodium cooled reactor.

Random Variable	**Units**	**Mean**	**Standard Dev.**
λ_1	s^{-1}	1.24E-02	6.20e-04
λ_2	s^{-1}	3.05E-02	1.52e-03
λ_3	s^{-1}	1.11E-01	5.55e-03
λ_4	s^{-1}	3.01E-01	1.50e-02
λ_5	s^{-1}	1.14E+00	5.70e-02
λ_6	s^{-1}	3.01E+00	1.50e-01
β_1		9.00E-05	4.50e-06
β_2		8.53E-04	4.26e-05
β_3		7.00E-04	3.50e-05
β_4		1.40E-03	7.00e-05
β_5		6.00E-04	3.00e-05
β_6		5.50E-04	2.75e-05
Λ	s	4.00E-07	2.00e-08
Ah	kW/K	2.50E+06	1.25e+05
M_c	kg	1.16E+03	5.84e+01
M_f	kg	9.67E+03	4.83e+02
c_{pc}	$J/kg \cdot K$	1.20E+03	6.00e+01
c_{pf}	$J/kg \cdot K$	5.00E+02	2.50e+01
v	m/s	7.50E+00	3.75e-01
α_d	pcm/K	6.87E-06	3.43e-07
α_c	pcm/K	1.23E-06	6.15e-08
ρ_{max}		4.19E-04	2.09e-05

Figure 3.4: Fuel temperature transient resulting from a half sawtooth reactivity insertion. All parameters in the coupled point kinetics/lumped thermal hydraulics equations are held at their mean values.

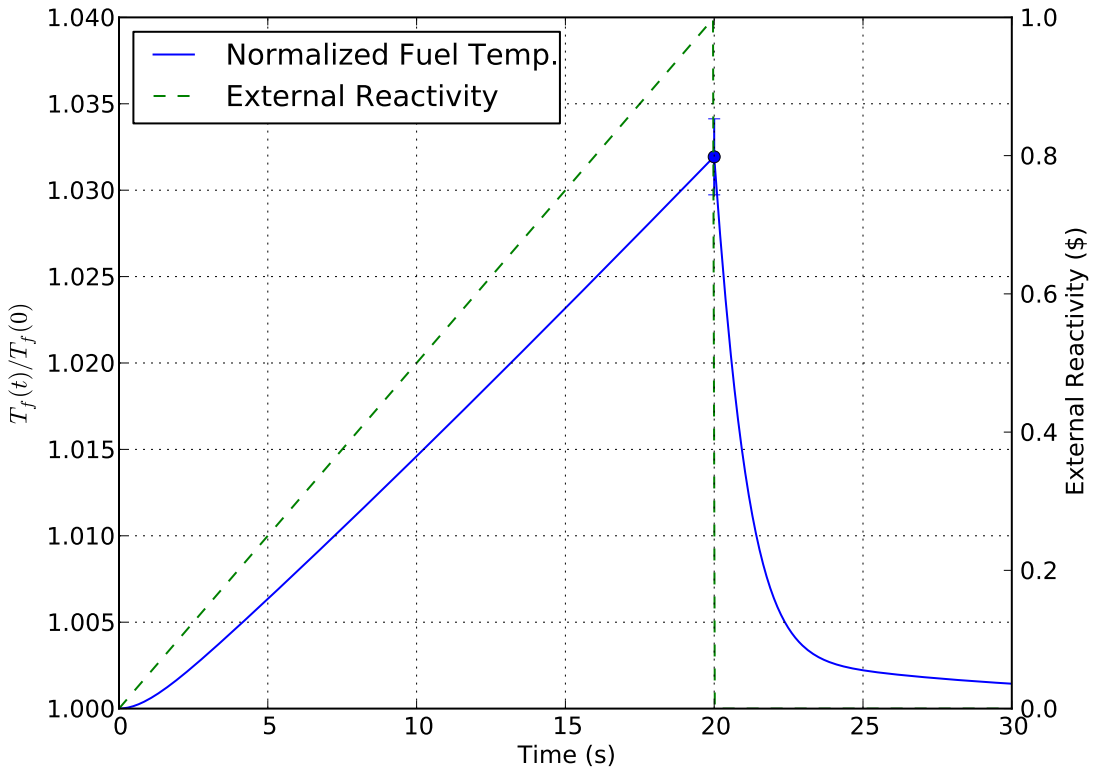

3.2.2 Analysis

An adaptive reduced order model, whose formulation is summarized in Algorithm 7, will be created for the problem described in section 3.2.1. The reduced order model will be investigated for its ability to reproduce statistics of interest by comparing its results with those obtained from sampling the true function. As described in Algorithm 7, the first step in creating a reduced order model for the maximum fuel temperature is to construct all first order components in the anchored-ANOVA decomposition and to identify the important ones. The sparse grids comprising the reduced order model are assumed to be converged when the maximum hierarchical surplus for a given level is less than 10^{-5}. Consequently, at least five digits of accuracy are expected. Important dimensions are those whose normalized sensitivity index in Eq. 2.54 exceeds 5%.

From Figure 3.5 the "important" variables are identified to be Ah, α_d, and ρ_{max}. Collec-

tively these three "important" random variables comprise 82% of the total sensitivity. The

Figure 3.5: Normalized sensitivity indices for all random variables comprising the coupled point kinetics/lumped thermal hydraulics equations. The effects of all β_k and λ_k have been lumped into single β a λ effects, respectively.

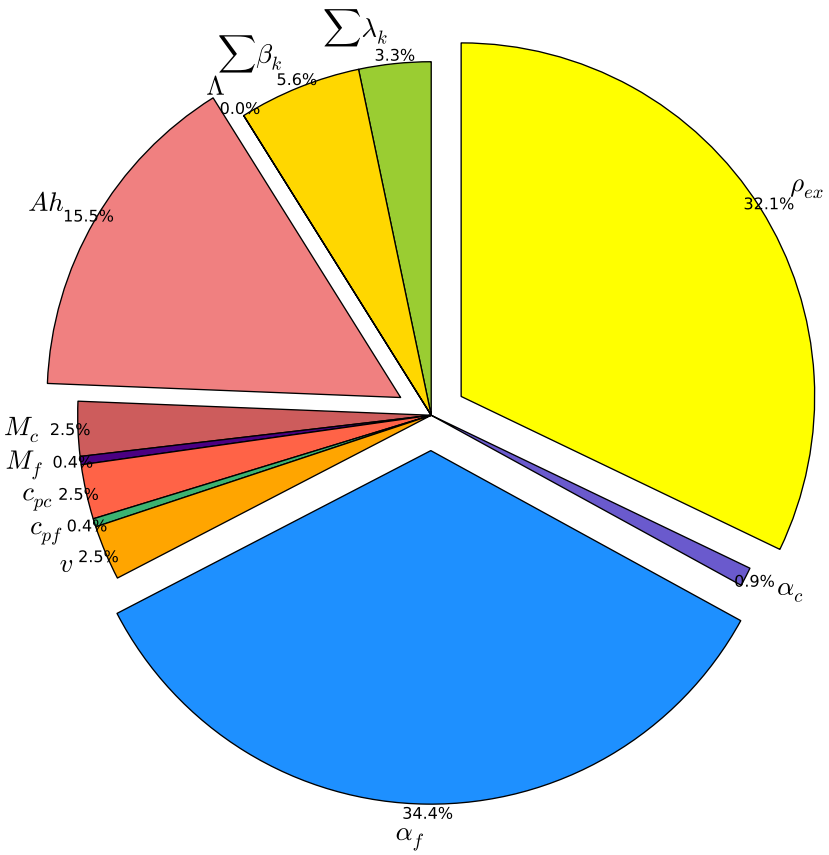

indication that the maximum fuel temperature is sensitive to the heat transfer Ah from fuel to coolant is not surprising since in Eq. 3.8 the fuel temperature is directly proportional to Ah. Further, the random variables ρ_{max} and α_d determine the slope of the increase in fuel temperature, as seen in Figure 3.4, and so a strong sensitivity to these random variables is expected. The sensitivity of the maximum fuel temperature to α_c is not as great since the increase in coolant temperature during the transient is significantly smaller than the rise in fuel temperature. Relatively weak sensitivity to M_f and c_{pf} can perhaps be attributed to cancellation of error since these two variables are multiplied together.

With only three random variables deemed as "important" only three second order anchored-ANOVA components must be built for the reduced order model. Neglecting any convergence criteria, third order component describing the interaction effects among the three important random variables is also built. A summary of the total number of function evaluations needed to construct the adaptive reduced order model for the maximum fuel temperature is shown in Figure 3.6. The Gauss-Patterson scheme required almost twice as many

Figure 3.6: Number of knots needed to adaptively construct a reduced order model for the maximum fuel temperature in both the Clenshaw-Curtis and Gauss-Patterson schemes. Boxed values state the standard deviation calculated at each level.

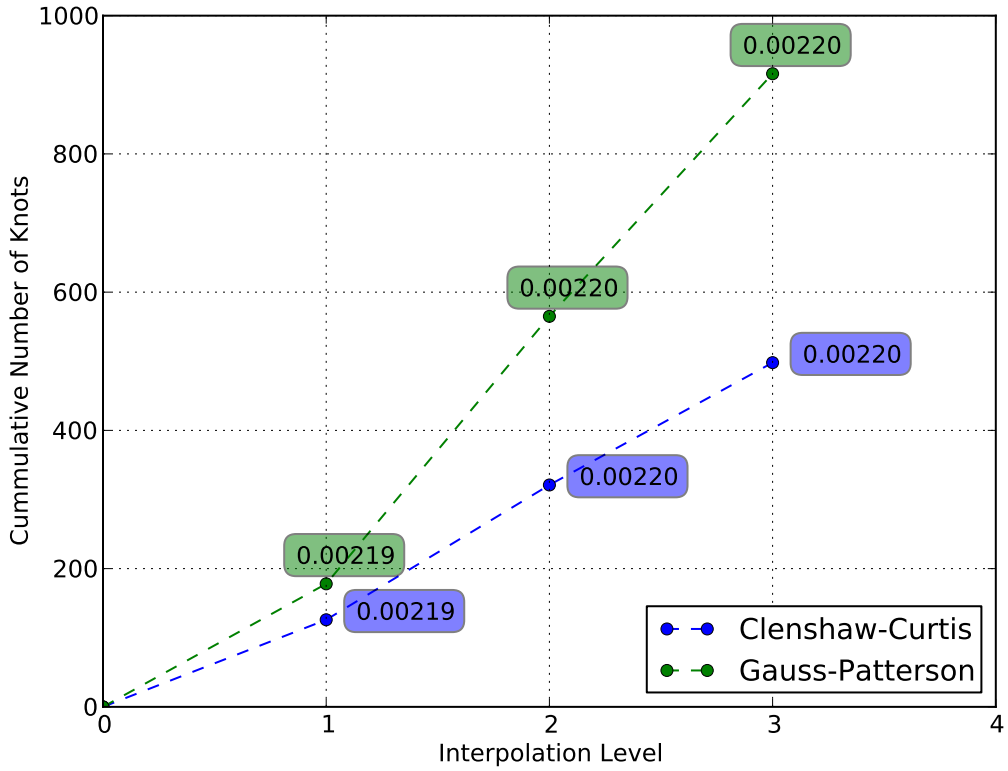

knots as Clenshaw-Curtis to adaptively build the reduced order model. From Figure 3.6 it's clear that the reduced order model consisting of only one dimensional components is effectively just as accurate as the full model, but requiring only 126 function evaluations to build using Clenshaw-Curtis. To see how well the reduced order models are able to reproduce the mean and variance of the true function Monte Carlo simulation is utilized. The models produced using anchored-ANOVA decomposition with superposition dimensions of one and three are sampled along with the true function. Mean, variance, and pertinent

99% confidence intervals for the sampling are summarized in Table 3.5. A total of 1000 samples were used for each method, each using the same random numbers. As evidenced

Table 3.5: Mean and variance data for the maximum fuel temperature achieved during transient obtained using Monte Carlo sampling. The same random numbers were used for all 1000 samples for each method.

Method	**Mean**	**99% CI**	**Standard Dev.**	**99% CI**
1D ANOVA CC	1.03193	(1.03175, 1.03211)	0.002187	(0.002068, 0.002320)
All ANOVA CC	1.03193	(1.03175, 1.03211)	0.002196	(0.002076, 0.002330)
1D ANOVA GP	1.03193	(1.03175, 1.03211)	0.002187	(0.002068, 0.002320)
All ANOVA GP	1.03193	(1.03175, 1.03211)	0.002196	(0.002076, 0.002330)
True Function	1.03193	(1.03175, 1.03211)	0.002196	(0.002076, 0.002330)

in Table 3.5 the statistical results for each method are consistent. While the reduced order model with superposition dimension of three is able to replicate the Monte Carlo results to five significant figures, the expected accuracy, the order-one superposition model is slightly short. Of course, this is due to the absence of higher order components. However, the proximity of the order-one superposition model's results to the true results indicate that for this problem the higher order components do not have a significant impact. To further verify the ability of the reduced order models to accurately reproduce basic statistical moments, the probability distributions for the normalized maximum fuel temperature produced by each model are compared in Figure 3.7. All of the tested reduced order models are able to reproduce the Gaussian probability distribution for the normalized maximum fuel temperature.

As done in section 3.1.2, a sensitivity analysis will be completed for the reduced order model and compared to the normalized sensitivity coefficients obtained using central differencing. From Table 3.6 notice that the largest sensitivity coefficients are those of the random variables deemed "important" using the adaptive reduced order model algorithm. Only the sensitivity coefficients for the Clenshaw-Curtis sparse grid are shown in Table 3.6 since the Gauss-Patterson sparse grid returns identical results. The normalized sensitivity coefficients calculated using the reduced order models are the same as those calculated using central differencing to the expected number of significant digits.

3.3 TMI Minicore

3.3.1 Problem Statement

The previous two problems dealt with relatively simple functions that don't require industrial engineering codes to solve. However, the main intention of this thesis is to construct

Figure 3.7: Histograms produced by sampling the true function, order-one superposition reduced order model, and the full adaptive reduced order model.

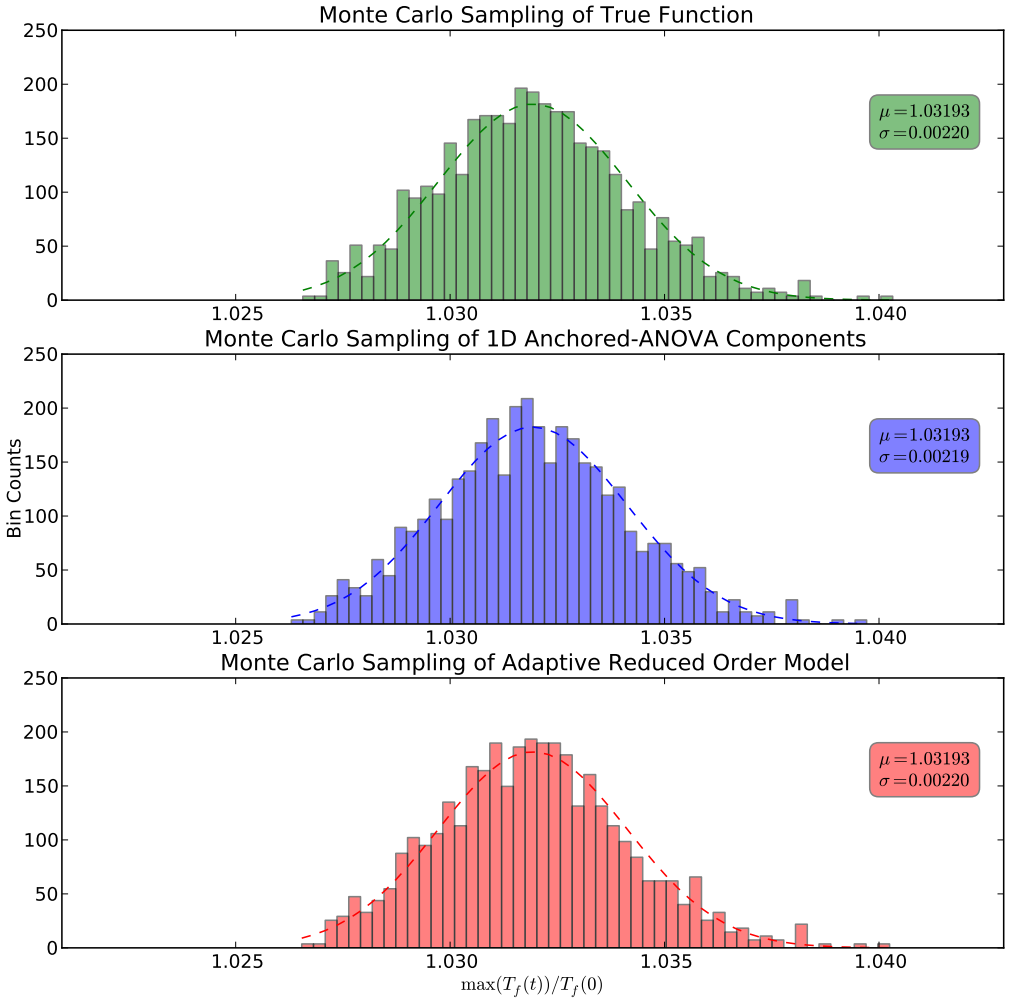

reduced order models for computer codes that aim to model large and complex engineering systems. Interaction with such computer codes consist of input and output files; the governing equations and their solvers are rarely seen. The primary purpose of this demonstration problem is to show that the same algorithms applied to analyze the previous problems are also functional when applied to engineering computer codes.

In this demonstration problem the reactor core simulator code PARCS [14] is applied to the TMI minicore described in the first phase of the UAM Benchmark [32]. The mini-

Table 3.6: Normalized sensitivity coefficients of the maximum fuel temperature to random variables.

Random Variable	1D ANOVA CC	All ANOVA CC	Central Diff.
λ_1	3.7894E-05	3.7894E-05	3.7895E-05
λ_2	7.0387E-04	7.0387E-04	7.0387E-04
λ_3	8.4244E-04	8.4244E-04	8.4215E-04
λ_4	9.7308E-04	9.7309E-04	9.7379E-04
λ_5	1.1572E-04	1.1572E-04	1.1607E-04
λ_6	4.4638E-05	4.4639E-05	4.0498E-05
β_1	-3.2992E-04	-3.2992E-04	-3.2976E-04
β_2	-2.6582E-03	-2.6582E-03	-2.6616E-03
β_3	-1.1953E-03	-1.1953E-03	-1.2040E-03
β_4	-1.0129E-03	-1.0129E-03	-1.0232E-03
β_5	-1.1689E-04	-1.1689E-04	-1.1810E-04
β_6	-4.0718E-05	-4.0718E-05	-4.1134E-05
Λ	-8.9294E-08	-8.9295E-08	-8.9364E-08
Ah	1.2553E-02	1.2553E-02	1.2584E-02
M_c	1.8753E-03	1.8753E-03	1.8716E-03
M_f	-3.6695E-04	-3.6695E-04	-3.6360E-04
c_{pc}	1.8753E-03	1.8753E-03	1.8903E-03
c_{pf}	-3.6695E-04	-3.6695E-04	-3.5976E-04
v	1.8838E-03	1.8839E-03	1.9177E-03
α_d	-2.6655E-02	-2.6656E-02	-2.6625E-02
α_c	8.4387E-04	8.4387E-04	8.7194E-04
ρ_{max}	3.1164E-02	3.1164E-02	3.1272E-02

core problem consists of a three-by-three fuel assembly configuration with reflector blocks placed around the assemblies, as seen in Figure 3.8. In the minicore the central assembly is rodded while the periphery fuel assemblies are unrodded. Vacuum boundary conditions are applied. The few-group, homogenized cross section description for each fuel assembly consists of transport, absorption, nu-fission, and scatter cross sections along with values for ADFs. For a two-group problem the total number of cross sections to describe an assembly is nine. Since the homogenized reflector region does not support fission only seven homogenized cross sections are required to describe it. Consequently, to model the minicore configuration in Fig. 3.8 in PARCS a total of twenty five homogenized, two-group cross sections are needed.

In order to study the effects of the uncertainties inherent in the few-group cross sections on output parameters of interest in PARCS, a few-group covariance matrix is necessary. The few-group covariance matrix is obtained using the 'two-step' method depicted in Fig.

Figure 3.8: TMI minicore configuration used for analysis, as defined in the UAM Benchmark specifications.

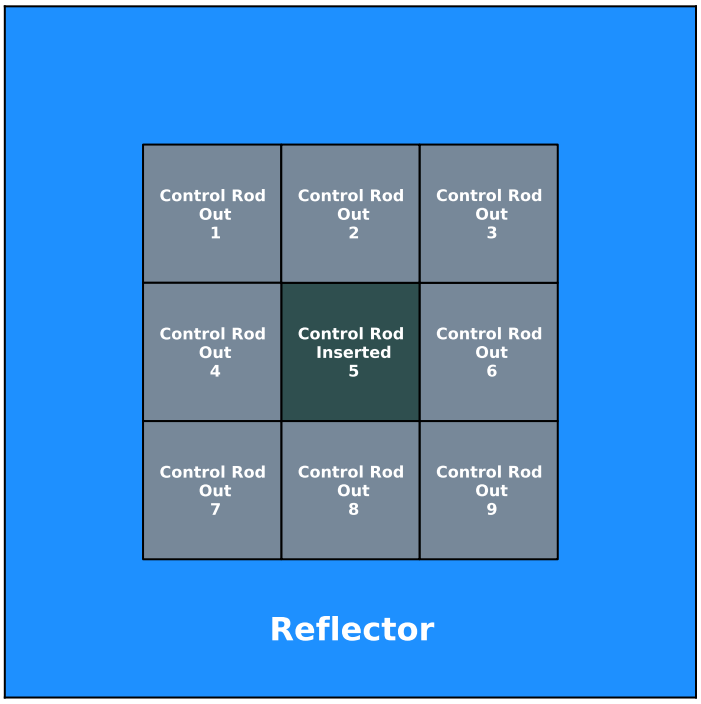

1.1. A total of 300 transport calculations with perturbed multigroup cross sections were executed to generate the few-group covariance matrix. In the previous example problems only one output parameter was investigated at a time. However, recall in the discussion of the Smolyak algorithm that interpolation is only performed on the random space. The objective function is evaluated at each abscissa in the random space, returning an output that can still be a function of physical space. In this case the hierarchical surplus is no longer one dimensional. Rather, the hierarchical surplus in Eq. 2.36 is rewritten as,

$$f(\mathbf{x}, x_{j_1}^{i_1}, \ldots, x_{j_d}^{i_d}) - A(q-1,d)(\mathbf{x}, x_{j_1}^{i_1}, \ldots, x_{j_d}^{i_d}) \tag{3.13}$$

where $\mathbf{x} \in \mathscr{D}$ is a coordinate in the spatial domain. When the objective function is a function of spatial coordinates the Smolyak algorithm approximates the function as a linear combination of vectors, the linear weights still being tensor products of basis functions for the random space. To determine the mean and variance of a reduced order model approx-

imation of some space-dependent objective function the L_2 norm is taken over the spatial domain $\mathscr{D}$. Similarly, to identify important dimensions using the sensitivity coefficient defined in Eq. 2.54 the L_2 norm is taken of $\eta_i(\mathbf{x})$.

The problem in this section considers the core box power distribution of the minicore in Fig. 3.8 and consequently, the objective function is space dependent. For each simulation in PARCS a vector of length nine is returned with each entry containing the relative box power in the fuel assemblies. The box powers are calculated such that the average of all nine entries is identically equal to unity. In the PARCS output file the box powers are only given to four digits of accuracy and therefore roundoff error in this problem warrants some attention.

3.3.2 Analysis

In this analysis a pure 'two-step' approach is used to compare the results obtained using a reduced order model for the box powers output in PARCS. For the 'two-step' approach a few group covariance matrix is constructed and sampled 500 times, with each sample containing perturbed few group cross sections. Each cross section set is propagated through the PARCS code and the box powers for the fuel assemblies are extracted from the output file. Ultimately, 500 box power outputs are analyzed statistically to obtain correlations, means, and variances. The same few group covariance matrix is used to sample the reduced order model for the box powers.

To build a reduced order model, Algorithm 7 is applied with a hierarchical surplus threshold of 10^{-4} since the PARCS box powers are only output to four decimal places. Consequently, roundoff error may accumulate in the fourth decimal point of the reduced order model. A total of 123 executions of PARCS were required to construct all single order components of the reduced order model using Clenshaw-Curtis abscissas. Due to the geometry of the TMI minicore, 1/8 symmetry is expected in the box power results. Consequently, only fuel assemblies one, four and five are investigated, as defined in Fig. 3.8. Sampling results for the mean and standard deviation for the true box power PARCS model and the reduced order model are summarized in Tables 3.7 and 3.8, respectively. As always, the same random numbers are used to produce each sample when comparing two different methods. The results are identical in all cases to four significant digits and in most cases, to five significant digits. In the reduced order model results notice that the standard deviation for assembly six is slightly off in the fourth decimal place when compared to assemblies two, four, and eight. The standard deviation should be equal in these four assemblies due to symmetry, indicating the presence of roundoff error.

Table 3.7: Mean and standard deviation data for TMI minicore box powers where PARCS code is used as objective function. A total of 500 samples were used. Assembly numbers correspond to Fig. 3.8.

Assembly	Mean	99% CI	Standard Dev.	99% CI
1	0.8387	(0.8386, 0.8388)	0.0007	(0.0006, 0.0008)
2	1.1499	(1.1498, 1.1500)	0.0011	(0.0010, 0.0012)
3	0.8387	(0.8386, 0.8388)	0.0007	(0.0006, 0.0008)
4	1.1499	(1.1498, 1.1500)	0.0011	(0.0010, 0.0012)
5	1.0453	(1.0450, 1.0456)	0.0027	(0.0025, 0.0029)
6	1.1499	(1.1498, 1.1500)	0.0011	(0.0010, 0.0012)
7	0.8387	(0.8386, 0.8388)	0.0007	(0.0006, 0.0008)
8	1.1499	(1.1498, 1.1500)	0.0011	(0.0010, 0.0012)
9	0.8387	(0.8386, 0.8388)	0.0007	(0.0006, 0.0008)

Table 3.8: Mean and standard deviation data for TMI minicore box powers where the objective function is a reduced order model for PARCS containing only 1D components. A total of 500 samples were used. Assembly numbers correspond to Fig. 3.8.

Assembly	Mean	99% CI	Standard Dev.	99% CI
1	0.8387	(0.8386, 0.8388)	0.0007	(0.0006, 0.0008)
2	1.1500	(1.1499, 1.1501)	0.0012	(0.0011, 0.0013)
3	0.8387	(0.8386, 0.8388)	0.0007	(0.0006, 0.0008)
4	1.1500	(1.1499, 1.1501)	0.0012	(0.0011, 0.0013)
5	1.0455	(1.0452, 1.0458)	0.0027	(0.0025, 0.0029)
6	1.1500	(1.1499, 1.1501)	0.0011	(0.0010, 0.0012)
7	0.8387	(0.8386, 0.8388)	0.0007	(0.0006, 0.0008)
8	1.1500	(1.1499, 1.1501)	0.0012	(0.0011, 0.0013)
9	0.8387	(0.8386, 0.8388)	0.0007	(0.0006, 0.0008)

Adding higher order components in accordance with Algorithm 7 did not improve the statistics of the reduced order model. For the purposes of uncertainty quantification the reduced order model consisting entirely of 1D components is sufficient for this problem. The bivariate distributions for the box powers for all combinations of assemblies one, four, and five are given in Fig. 3.9. For each case in Fig. 3.9 the bivariate distributions are obtained by sampling the reduced order model and PARCS. Variations between the overlaid distributions can be attributed to roundoff error. A decrease in the box power of assembly five is equivalent to an increase in the absorption of the assembly's control rods, which effectively shifts the neutron flux away from the central assembly. Consequently, a negative correlation is expected between assemblies one and five and between assemblies one and four. Indeed, statistical sampling has the Pearson correlation coefficient for the box powers

of assemblies one and four to be -0.83 and -0.84 between assemblies one and five. However, negative correlation coefficients between assembly one and assemblies four and five implies a positive correlation coefficient between assemblies four and five. The positive correlation coefficient of $+0.40$ between assemblies four and five is evident in Fig. 3.9.

3.4 General Observations

Before moving on to a large-scale engineering system a few general observations regarding the application of collocation-based reduced order models to the uncertainty quantification of the reactor systems described are in order. Primarily, the demonstration problems indicate that use of only 1D components in the anchored-ANOVA expansion provides a very good approximation to the true system under investigation. From a computational point of view, 1D components are cheap to build and their quantity is equal to the number of random variables modeled. Higher order components generally require higher levels of interpolation and so their construction should be minimized if possible. As mentioned in [42], the interaction effects between random variables for most realistic physical systems have a negligible effect on outputs of interest.

Nevertheless, if multivariate components are needed algorithm 7 is able to identify the combination of components most likely to affect the output, which offers significant computational savings. For example, if all components of two random variables were to be included in the anchored-ANOVA expansion then 4950 two-dimensional sparse grid interpolants would need to be built. However, if only 5 of the 100 variables are deemed "important" by algorithm 7 then only 10 two-dimensional sparse grid interpolants will be built. Not to mention, identification of variables that most affect the variability in some computer code output of interest offers insight into the physical system under consideration. It should be reemphasized that components of the anchored-ANOVA used to build reduced order models do not represent the order of effects on the output. Even the 1D component functions can model nonlinear behavior as discussed in section 2.3.2. Rather, the multivariate components describe the affect of input variables upon some output when acting together.

For the demonstration problems investigated in this chapter, the Clenshaw-Curtis collocation abscissas performed significantly better than Gauss-Patterson. The Clenshaw-Curtis knots offered effectively the same convergence rates as Gauss-Patterson with far fewer function evaluations. Not to mention, Clenshaw-Curtis knots are much easier to generate.

Figure 3.9: Multivariate distributions for the box powers of two assemblies. Dashed distributions were obtained by sampling the reduced order model consisting of only 1D components.

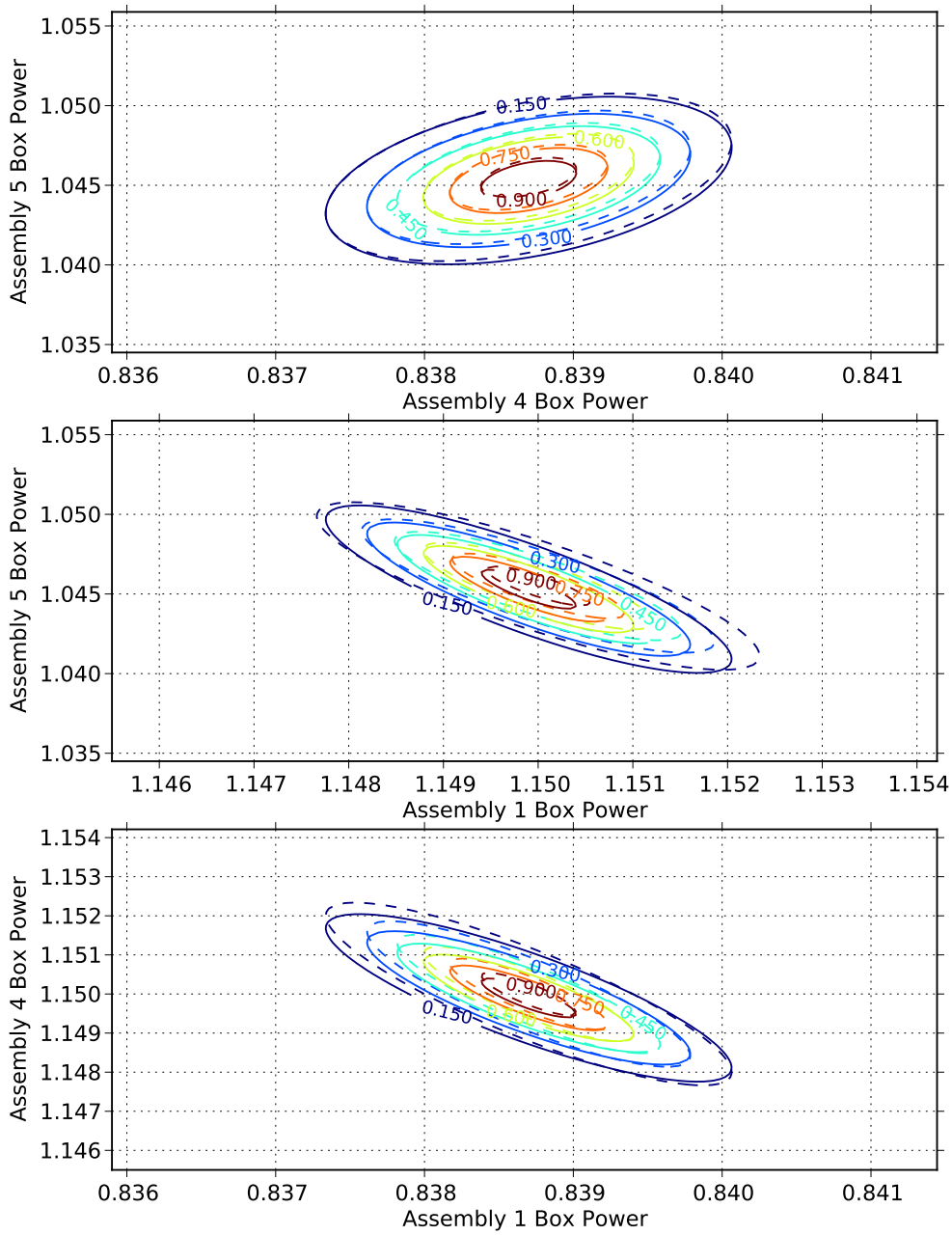

BIBLIOGRAPHY

[1] H.S. Abdel-Khalik and P.J. Turinsky. Evaluation of core attributes uncertainties due to input data uncertainties. volume 92 of *Transactions of the American Nuclear Society*, San Diego, CA, 2005.

[2] Nitin Agarwal and N.R. Aluru. A domain adaptive stochastic collocation approach for analysis of mems under uncertainties. *Journal of Computational Physics*, 228:7662–7688, 2009.

[3] John K. Au. *An Ab Initio Approach to the Inverse Problem-based Design of Photonic Bandgap Devices*. PhD thesis, California Institute of Technology, 2007.

[4] D. Ayres, M.M.R. Williams, and M.D. Eaton. Time and static eigenvalues of the stochastic transport equation by the methods of polynomial chaos. *Progress in Nuclear Energy*, 67:33–55, 2013.

[5] Volker Barthelmann, Erich Novak, and Klaus Ritter. High dimensional polynomial interpolation on sparse grids. *Advances in Computational Mathematics*, 12:273–288, 2000.

[6] Jean-Paul Berrut and Lloyd N. Trefethen. Barycentric lagrange interpolation. *SIAM Review*, 46(3):501–517, 2004.

[7] S.M. Bowman. Scale 6: Comprehensive nuclear safety analysis code system. *Nuclear Technology*, 174(2):126–148, 2011.

[8] George Box. Evolutionary operation: A method for increasing industrial productivity. *Journal of the Royal Statistical Society*, 6(2):81–101, 1957.

[9] John Boyd. *Chebyshev and Fourier Spectral Methods*. Dover Publications, 2 edition, 2001.

[10] John P. Boyd. *Chebyshev and Fourier Spectral Methods*. Dover Publications, 2 edition, 2001.

[11] T. Bui-Thanh, K. Willcox, and O. Ghattas. Model reduction for large-scale systems with high-dimensional parametric input space. *SIAM Journal on Scientific Computing*, 30(6):3270–3288, 2008.

[12] John Burkardt. Sparse grid collocation for uncertainty quantification. SCALA, Louisiana State University, 2012.

[13] Philip Davis and Philip Rabinowitz. *Methods of Numerical Integration*. Dover, 2007.

[14] Thomas Downar. Parcs: Purdue advanced reactor core simulator. Proceedings of the International Conference on the New Frontiers of Nuclear Technology, Seoul, South Korea, 2002.

[15] James Duderstadt and Louis Hamilton. *Nuclear Reactor Analysis*. John Wiley and Sons, 1976.

[16] D. Eardley. Quantification of margins and uncertainties. Technical report, MITRE Corporation, March 2005.

[17] Erin D. Fichtl and Anil K. Prinja. The stochastic collocation method for radiation transport in random media. *Journal of Quantitative Spectroscopy and Radiative Transfer*, 112(4):646–659, 2011.

[18] Alexander Forrester, Andras Sobester, and Andy Keane. *Engineering Design via Surrogate Modelling*. Wiley and Sons, 2008.

[19] A. Gandini. Implicit and explicit higher order perturbation methods for nuclear reactor analysis. *Nuclear Science and Engineering*, 67, 1978.

[20] Zhen Gao and Jan S. Hesthaven. On anova expansions and strategies for choosing the anchor point. *Applied Mathematics and Computation*, 217:3274–3285, 2010.

[21] Zhen Gao and Jan S. Hesthaven. Efficient solution of orindary differential equations with high-dimensional parameterized uncertainty. *Communications in Computational Physics*, 10(2):253–278, 2011.

[22] Roger Ghanem and P. D. Spanos. Polynomial chaos in stochastic finite elements. *Journal of Applied Mechanics*, 57(1):197–202, 1990.

[23] L. Gilli, D. Lathouwers, J.L. Kloosterman, and T.H. van der Hagen. Application of sensitivity analysis to a simplified coupled neutronic thermal-hydraulics transient in a fast reactor using adjoint techniques. In *International Conference on Mathematics and Computational Methods Applied to Nuclear Science and Engineering*, Rio de Janiero, Brazil, May 2011. American Nuclear Society.

[24] L. Gilli, D. Lathouwers, J.L. Kloosterman, and T.H. van der Hagen. Performing uncertainty analysis of a nonlinear point-kinetics/lumped paremeters problem using polynomial chaos techniques. *Annals of Nuclear Energy*, 40:35–44, 2012.

[25] A.A. Giunta, J.M. McFarland, L.P. Swiler, and M.S. Eldred. The promise and peril of uncertainty quantification using response surface approximations. *Structure and Infrastructure Engineering*, 2(3-4):175–189, 2006.

[26] J.C. Helton and F.J. Davis. Latin hypercube sampling and the propagation of uncertainty in analysis of complex systems. *Reliability Engineering and System Safety*, 81:23–69, 2003.

[27] Peter Henrici. *Essentials of Numerical Analysis with Pocket Calculator Demonstrations*. John Wiley and Sons, 1982.

[28] Markus Holtz. *Sparse Grid Quadrature in High Dimensions with Applications in Finance and Insurnance*. Springer, 2011.

[29] C. Housiadas. Lumped paramaters analysis of coupled kinetics and thermal-hydraulics for small reactors. *Annals of Nuclear Energy*, 29:1315–1325, 2002.

[30] Gianluca Iaccarino. Uncertainty quantification in computational science. Lehrstuhl fr Aerodynamik und Strmungsmechanik, Technische Universitt Mnchen, 2011.

[31] Edward H. Isaaks and Mohan Srivastava. *An Introduction to Applied Geostatistics*. Oxford University Press, 1990.

[32] K. Ivanov, M. Avramova, I. Kodeli, and E. Sartori. Benchmark for uncertainty analysis in modeling for design, operation and safety analysis of lwrs. Technical report, Nuclear Energy Agency, 2007.

[33] M.A. Jessee, H.S. Khalik, and P.J. Turinsky. Evaluation of bwr core attributes uncertainties due to multi- group cross section uncertainties. In *Joint International Topical Meeting on Mathematics and Computation and Supercomputing in Nuclear Applications*, Monterey, CA, April 2007. American Nuclear Society.

[34] M.A. Jessee, P.J. Turinsky, and H.S. Abdel-Khalik. Many-group cross-section adjustment techniques for boiling water reactor adaptive simulation. *Nuclear Science and Engineering*, 169:40–55, 2011.

[35] H.F. Kaiser and K. Dichman. Sample and population score matrices and sample correlation matrices from an arbitrary population correlation matrix. *Psychometrica*, 27(2):179–182, 1962.

[36] S. Kirkpatrick, C. D. Gelatt Jr., and M. P. Vecchi. Optimization by simulated annealing. *Science*, 220:671–680, 1983.

[37] M. Klein, L. Gallner, B. Krzykacz-Hausmann, A. Pautz, and W. Zwermann. Influence of nuclear data covariance on reactor core calculations. *Kerntechnik*, 3:174–78, 2011.

[38] Andreas Klimke and Barbara Wohlmuth. Peicewise multilinear hierarchical sparse grid interpolation in matlab. *ACM Transactions on Mathematical Software*, 31(4):561–579, 2005.

[39] Genyuan Li, Sheng-Wei Wang, and Herschel Rabitz. High dimensional model representations: Concepts and applications. *Journal of Physical Chemistry A*, 105:7765–7777, 2001.

[40] Meilin Liu, Zhen Gao, and Jan Hesthaven. Adaptive sparse grid algorithms with applications to electromagnetic scattering under uncertainty. *Applied Numerical Mathematics*, 61:24–37, 2011.

[41] Xiang Ma and Nicholas Zabaras. An adaptive hierarchical sparse grid collocation algorithm for the solution of stochastic differential equations. *Journal of Computational Physics*, 228:3084–3113, 2009.

[42] Xiang Ma and Nicholas Zabaras. An adaptive high-dimensional stochastic model representation technique for the solution of stochastic partial differential equations. *Journal of Computational Physics*, 229:3884–3915, 2009.

[43] O.P Le Maitre and Omar Knio. *Spectral Methods for Uncertainty Quantification: With Applications to Computational Fluid Dynamics*. Springer, 2010.

[44] Max D. Morris. Factorial sampling plans for preliminary computational experiments. *Technometrics*, 33(2):161–174, 1991.

[45] Max D. Morris and Toby J. Mitchell. Exploratory designs for computational experiments. *Journal of Statistical Planning and Inference*, 43:381–402, 1995.

[46] Brent Oksendal. *Stochastic Differential Equations: An Introduction with Applications*. Springer-Verlag, 6 edition, 2005.

[47] Jerome Sacks, William Welch, Toby Mitchell, and Henry Wynn. Design and analysis of computer experiments. *Statistical Science*, 4(4):409–435, 1989.

[48] H.E. Salzer. Lagrangian interpolation at the chebyshev points $x_{n,v} = \cos(v\pi/n)$. *The Computer Journal*, 15(2):156–159, 1972.

[49] Sergei A. Smolyak. Quadrature and interpolation formulas for tensor products of certain classes of functions. *Soviet Math. Dokl.*, 4:240–243, 1963.

[50] L. Swiler, R. Slepoy, and A.A. Giunta. Evaluation of sampling methods in constructing response surface approximations. In *SDM non-Deterministic Approaches Conference*. American Institute of Aeronautics and Astronautics, May 2006.

[51] Lloyd Trefethen. Is gaussian quadrature better than clenshaw-curtis? *SIAM Review*, 50(1):67–87, 2008.

[52] Lloyd Trefethen. *Approximation Theory and Approximation Practice*. SIAM, 2012.

[53] M.L. Williams. Perturbation theory for reactor analysis. In *CRC Handbook of Nuclear Reactor Calculations*, pages 63–188. CRC Press, 1986.

[54] M.L. Williams, J.C. Gehin, and W.S. Yang. Combining mc^2-2 and scale cross section methods to process nuclear data for gnep. In *International Conference on Reactor Physics, Nuclear Power: A Sustainable Resource*, Interlaken, Switzerland, September 2008.

[55] M.L. Williams, G. Ilas, M.A. Jessee, B.T. Rearden, D. Wiarda, W. Zwermann, L. Gallner, M. Klein, B. Krzykacz-Hausmann, and A. Pautz. A statistical sampling method for uncertainty analysis with scale and xsusa. *Nuclear Technology*, 183(3):515–526, 2012.

[56] M.M.R. Williams. Polynomial chaos functions and stochastic differential equations. *Annals of Nuclear Energy*, 33(9):774–785, 2006.

[57] M.M.R. Williams. Polynomial chaos functions and neutron diffusion. *Nuclear Science and Engineering*, 155(1):109–118, 2007.

[58] Dongbin Xiu and Jan S. Hesthaven. High-order collocation methods for differential equations with random inputs. *SIAM Journal of Scientific Computing*, 27:1118–1139, 2005.

[59] A. Yankov, B.S. Collins, M.A. Jessee, and T.J. Downar. A generalized adjoint approach for quantifying reflector assembly discontinuity factor uncertainties. In *Advances in Reactor Physics*, Knoxville, TN, April 2012. American Nuclear Society.

[60] Artem Yankov, Benjamin Collins, and Markus Klein. A two-step approach to uncertainty quantification of core simulators. *Science and Technology of Nuclear Installations*, 2012.